acid metabolism and resistance to oxidative stress. *Mol Cell* **11**: 619–633

Hershko A, Ciechanover A (1998) The ubiquitin system. *Annu Rev Biochem* **67**: 425–479

Hodgins RR, Ellison KS, Ellison MJ (1992) Expression of a ubiquitin derivative that conjugates to protein irreversibly produces phenotypes consistent with a ubiquitin deficiency. *J Biol Chem* **267**: 8807–8812

Ichimura Y, Kirisako T, Takao T, Satomi Y, Shimonishi Y, Ishihara N, Mizushima N, Tanida I, Kominami E, Ohsumi M, Noda T, Ohsumi Y (2000) A ubiquitin-like system mediates protein lipidation. *Nature* **408**: 488–492

Jentsch S, Pyrowolakis G (2000) Ubiquitin and its kin: how close are the family ties? *Trends Cell Biol* **10**: 335–342

Johnson ES, Blobel G (1997) Ubc9p is the conjugating enzyme for the ubiquitin-like protein Smt3p. *J Biol Chem* **272**: 26799–26802

Johnson ES, Schwienhorst I, Dohmen RJ, Blobel G (1997) The ubiquitin-like protein Smt3p is activated for conjugation to other proteins by an Aos1p/Uba2p heterodimer. *EMBO J* **16**: 5509–5519

Kabeya Y, Mizushima N, Ueno T, Yamamoto A, Kirisako T, Noda T, Kominami E, Ohsumi Y, Yoshimori T (2000) LC3, a mammalian homologue of yeast Apg8p, is localized in autophagosome membranes after processing. *EMBO J* **19**: 5720–5728

Kamitani T, Nguyen HP, Yeh ET (1997) Preferential modification of nuclear proteins by a novel ubiquitin-like molecule. *J Biol Chem* **272**: 14001–14004

Klionsky DJ, Cregg JM, Dunn Jr WA, Emr SD, Sakai Y, Sandoval IV, Sibirny A, Subramani S, Thumm M, Veenhuis M, Ohsumi Y (2003) A unified nomenclature for yeast autophagy-related genes. *Dev Cell* **5**: 539–545

Klionsky DJ, Emr SD (2000) Autophagy as a regulated pathway of cellular degradation. *Science* **290**: 1717–1721

Komatsu M, Tanida I, Ueno T, Ohsumi M, Ohsumi Y, Kominami E (2001) The C-terminal region of an Apg7p/Cvt2p is required for homodimerization and is essential for its E1 activity and E1–E2 complex formation. *J Biol Chem* **276**: 9846–9854

Lammer D, Mathias N, Laplaza JM, Jiang W, Liu Y, Callis J, Goebl M, Estelle M (1998) Modification of yeast Cdc53p by the ubiquitin-related protein rub1p affects function of the SCFCdc4 complex. *Genes Dev* **12**: 914–926

Liakopoulos D, Doenges G, Matuschewski K, Jentsch S (1998) A novel protein modification pathway related to the ubiquitin system. *EMBO J* **17**: 2208–2214

Liu YC, Pan J, Zhang C, Fan W, Collinge M, Bender JR, Weissman SM (1999) A MHC-encoded ubiquitin-like protein (FAT10) binds noncovalently to the spindle assembly checkpoint protein MAD2. *Proc Natl Acad Sci USA* **96**: 4313–4318

Mizushima N, Noda T, Yoshimori T, Tanaka Y, Ishii T, George MD, Klionsky DJ, Ohsumi M, Ohsumi Y (1998) A protein conjugation system essential for autophagy. *Nature* **395**: 395–398

Nakamura M, Xavier RM, Tsunematsu T, Tanigawa Y (1995) Molecular cloning and characterization of a cDNA encoding monoclonal nonspecific suppressor factor. *Proc Natl Acad Sci USA* **92**: 3463–3467

Natsume T, Yamauchi Y, Nakayama H, Shinkawa T, Yanagida M, Takahashi N, Isobe T (2002) A direct nanoflow liquid chromatography–tandem mass spectrometry system for interaction proteomics. *Anal Chem* **74**: 4725–4733

Ohsumi Y (2001) Molecular dissection of autophagy: two ubiquitin-like systems. *Nat Rev Mol Cell Biol* **2**: 211–216

Osaka F, Kawasaki H, Aida N, Saeki M, Chiba T, Kawashima S, Tanaka K, Kato S (1998) A new NEDD8-ligating system for cullin-4A. *Genes Dev* **12**: 2263–2268

Pickart CM (2001) Mechanisms underlying ubiquitination. *Annu Rev Biochem* **70**: 503–533

Schwartz DC, Hochstrasser M (2003) A superfamily of protein tags: ubiquitin, SUMO and related modifiers. *Trends Biochem Sci* **28**: 321–328

Shintani T, Mizushima N, Ogawa Y, Matsuura A, Noda T, Ohsumi Y (1999) Apg10p, a novel protein-conjugating enzyme essential for autophagy in yeast. *EMBO J* **18**: 5234–5241

Tanaka K, Suzuki T, Chiba T (1998) The ligation systems for ubiquitin and ubiquitin-like proteins. *Mol Cells* **8**: 503–512

Tanida I, Komatsu M, Ueno T, Kominami E (2003) GATE-16 and GABARAP are authentic modifiers mediated by Apg7 and Apg3. *Biochem Biophys Res Commun* **300**: 637–644

Tanida I, Mizushima N, Kiyooka M, Ohsumi M, Ueno T, Ohsumi Y, Kominami E (1999) Apg7p/Cvt2p: a novel protein-activating enzyme essential for autophagy. *Mol Biol Cell* **10**: 1367–1379

Varshavsky A (1997) The ubiquitin system. *Trends Biochem Sci* **22**: 383–387

Walden H, Podgorski MS, Huang DT, Miller DW, Howard RJ, Minor Jr DL, Holton JM, Schulman BA (2003a) The structure of the APPBP1–UBA3–NEDD8–ATP complex reveals the basis for selective ubiquitin-like protein activation by an E1. *Mol Cell* **12**: 1427–1437

Walden H, Podgorski MS, Schulman BA (2003b) Insights into the ubiquitin transfer cascade from the structure of the activating enzyme for NEDD8. *Nature* **422**: 330–334

Yeh ET, Gong L, Kamitani T (2000) Ubiquitin-like proteins: new wines in new bottles. *Gene* **248**: 1–14

Developmental Cell, Vol. 6, 661–672, May, 2004, Copyright ©2004 by Cell Press

Skp2-Mediated Degradation of p27 Regulates Progression into Mitosis

Keiko Nakayama,[1,2,5] Hiroyasu Nagahama,[2,3,5] Yohji A. Minamishima,[2,3] Satoshi Miyake,[1,2] Noriko Ishida,[1,2,3] Shigetsugu Hatakeyama,[2,3] Masatoshi Kitagawa,[2,3] Shun-ichiro Iemura,[4] Tohru Natsume,[4] and Keiichi I. Nakayama[2,3,*]
[1]Division of Developmental Genetics
Center for Translational and Advanced Animal Research on Human Diseases
Tohoku University School of Medicine
Sendai, Miyagi 980-8575
Japan
[2]CREST
Japan Science and Technology Corporation (JST)
Kawaguchi, Saitama 332-0012
Japan
[3]Department of Molecular and Cellular Biology
Medical Institute of Bioregulation
Kyushu University
Fukuoka, Fukuoka 812-8582
Japan
[4]National Institute of Advanced Industrial Science and Technology (AIST)
Biological Information Research Center
Tokyo 135-0064
Japan

Summary

Although Skp2 has been thought to mediate the degradation of p27 at the G_1-S transition, *Skp2*$^{-/-}$ cells exhibit accumulation of p27 in S-G_2 phase with overreplication. We demonstrate that *Skp2*$^{-/-}$*p27*$^{-/-}$ mice do not exhibit the overreplication phenotype, suggesting that p27 accumulation is required for its development. Hepatocytes of *Skp2*$^{-/-}$ mice entered the endoduplication cycle after mitogenic stimulation, whereas this phenotype was not apparent in *Skp2*$^{-/-}$*p27*$^{-/-}$ mice. Cdc2-associated kinase activity was lower in *Skp2*$^{-/-}$ cells than in wild-type cells, and a reduction in Cdc2 activity was sufficient to induce overreplication. The lack of p27 degradation in G_2 phase in *Skp2*$^{-/-}$ cells may thus result in suppression of Cdc2 activity and consequent inhibition of entry into M phase. These data suggest that p27 proteolysis is necessary for the activation of not only Cdk2 but also Cdc2, and that Skp2 contributes to regulation of G_2-M progression by mediating the degradation of p27.

Introduction

The highly ordered progression of the cell cycle is achieved by a series of elaborate mechanisms that control the periodic expression of many regulatory proteins. One such regulatory protein is the Cdk inhibitor (CKI) p27. In normal cells, the amount of p27 is high during G_0 phase but rapidly decreases on the reentry of cells into G_1-S. Moreover, we and others have demonstrated that *p27*$^{-/-}$ mice are larger than normal mice and exhibit both multiple organ hyperplasia and a predisposition to the development of tumors (Fero et al., 1996; Kiyokawa et al., 1996; Nakayama et al., 1996).

The intracellular concentration of p27 is thought to be regulated predominantly by the ubiquitin-mediated proteolytic pathway (Pagano et al., 1995; Shirane et al., 1999). Degradation of p27 is promoted by its phosphorylation on Thr^{187} by the cyclin E-Cdk2 complex (Sheaff et al., 1997; Vlach et al., 1997; Montagnoli et al., 1999). Skp2, an F box protein that functions as the receptor component of an SCF ubiquitin ligase complex, binds to p27 only when Thr^{187} of this CKI is phosphorylated; such binding then results in the ubiquitylation and degradation of p27 (Carrano et al., 1999; Sutterluty et al., 1999; Tsvetkov et al., 1999). Skp2 also targets free cyclin E (not that complexed with Cdk2) for ubiquitylation (Nakayama et al., 2000). These biochemical observations are supported by genetic evidence showing that both p27 and free cyclin E accumulate to high levels in the cells of mice that lack Skp2 (Nakayama et al., 2000, 2001). The most obvious cellular phenotype of *Skp2*$^{-/-}$ mice is the presence of markedly enlarged, polyploid nuclei and multiple centrosomes, suggestive of an impairment in the mechanism that prevents endoreplication, in which the genomic DNA content of a cell is increased without cell division. In addition to p27 and free cyclin E, several other substrates have been proposed for Skp2. However, some of these potential substrates were found not to accumulate in cells from *Skp2*$^{-/-}$ mice, suggesting either that they are not bona fide Skp2 substrates or that functional redundancy allows for their ubiquitylation in the absence of Skp2.

Skp2 is almost undetectable or expressed at a low level in G_0 and early to mid-G_1 phase. It begins to accumulate during late G_1 phase, and its abundance is maximal during S and G_2 phases (Hara et al., 2001). The onset of Skp2 expression is unequivocally later than that of the degradation of p27 apparent at G_0-G_1. Moreover, p27 is exported from the nucleus to the cytoplasm at G_0-G_1 (Rodier et al., 2001; Ishida et al., 2002; Connor et al., 2003), whereas Skp2 is restricted to the nucleus (Miura et al., 1999). The discrepancies between the temporal and spatial patterns of p27 expression and those of Skp2 expression suggest the existence of an Skp2-independent pathway for the degradation of p27 at the G_0-G_1 transition. Indeed, the downregulation of p27 at G_0-G_1 occurs normally in *Skp2*$^{-/-}$ cells, but that in S and G_2 phases is impaired (Hara et al., 2001). These findings suggest that the major role of Skp2 might be to reduce the concentration of p27 during S and G_2 phases rather than at late G_1 phase.

To determine whether the accumulation of p27 is essential for the polyploidy and centrosome overduplication in *Skp2*$^{-/-}$ cells, we generated double mutant mice that lack both Skp2 and p27 genes. We now show that, although cyclin E accumulates in the cells of *Skp2*$^{-/-}$ *p27*$^{-/-}$ mice, the markedly enlarged, polyploid

*Correspondence: nakayak1@bioreg.kyushu-u.ac.jp
[5]These authors contributed equally to this work.

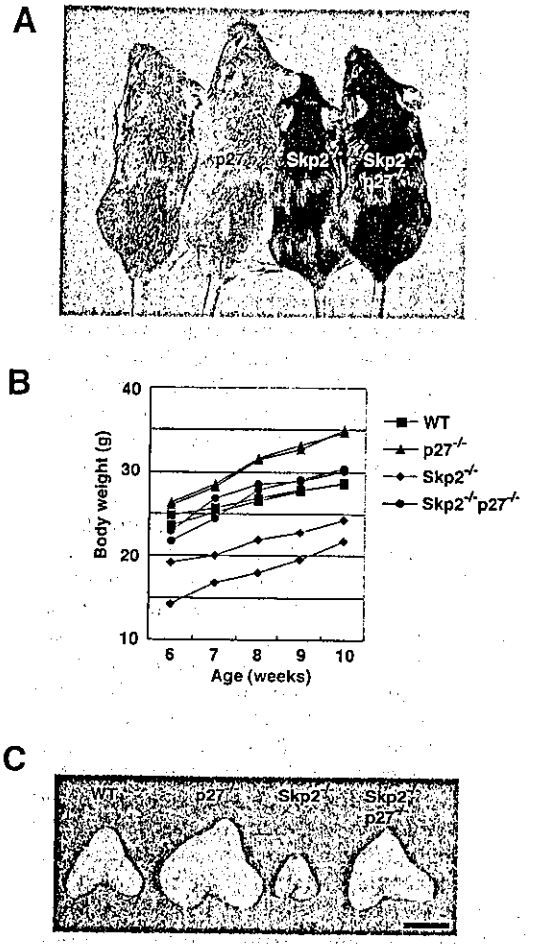

Figure 1. Body and Thymus Size in *Skp2*$^{-/-}$ *p27*$^{-/-}$ Mice

(A) Representative male wild-type (WT), *p27*$^{-/-}$, *Skp2*$^{-/-}$, and *Skp2*$^{-/-}$ *p27*$^{-/-}$ littermates at 8 weeks of age.

(B) Representative growth curves for male wild-type, *p27*$^{-/-}$, *Skp2*$^{-/-}$, and *Skp2*$^{-/-}$ *p27*$^{-/-}$ mice. Similar differences in body weight were apparent for female mice of the various genotypes (data not shown).

(C) Gross appearance of the thymus of male wild-type, *p27*$^{-/-}$, *Skp2*$^{-/-}$, and *Skp2*$^{-/-}$ *p27*$^{-/-}$ littermates at 8 weeks of age. Scale bar, 5 mm.

nuclei and multiple centrosomes associated with Skp2 deficiency are not evident in the double mutant mice. These data suggest that accumulation of p27 is primarily responsible for this cellular phenotype of *Skp2*$^{-/-}$ mice. We also demonstrate that the aberrant increase in p27 expression in *Skp2*$^{-/-}$ cells results in inhibition of the kinase activity of Cdc2 and a consequent block of entry into M phase. Our results thus indicate that Skp2 plays a crucial role in regulation of G_2-M progression by contributing to the ubiquitylation-mediated proteolysis of p27.

Results

Generation of Mice Lacking Both Skp2 and p27

To generate mice lacking Skp2 and p27, we crossed *Skp2*$^{+/-}$ *p27*$^{+/-}$ animals. As we previously described (Nakayama et al., 1996, 2000), the body size of *p27*$^{-/-}$ animals is larger and that of *Skp2*$^{-/-}$ mice is smaller than that of wild-type controls (Figures 1A and 1B). The body size of the *Skp2*$^{-/-}$ *p27*$^{-/-}$ double mutant was slightly larger than that of wild-type controls. We also examined the size of the thymus, which is one of the most affected organs in *Skp2*$^{-/-}$ or *p27*$^{-/-}$ mice; it is hyperplastic in *p27*$^{-/-}$ mice and atrophic in *Skp2*$^{-/-}$ mice (Figure 1C). As with body size, the thymus of *Skp2*$^{-/-}$ *p27*$^{-/-}$ mice was slightly larger than that of wild-type animals. In general, the *Skp2*$^{-/-}$ *p27*$^{-/-}$ mice appeared similar to *p27*$^{-/-}$ mice and exhibited phenotypes opposite to those of *Skp2*$^{-/-}$ mice. The observation that the *Skp2*$^{-/-}$ *p27*$^{-/-}$ double mutant appears similar but not identical to the *p27*$^{-/-}$ single mutant constitutes genetic evidence for the notion that, although p27 is the main target of Skp2, Skp2 may also mediate the ubiquitylation of other substrates.

Absence of Overreplication Phenotype in *Skp2*$^{-/-}$ *p27*$^{-/-}$ Mice

The most obvious cellular phenotype of *Skp2*$^{-/-}$ mice is the presence of markedly enlarged, polyploid nuclei and multiple centrosomes (Nakayama et al., 2000). To determine whether these characteristics are dependent on p27 accumulation, we examined liver, kidney, and lung cells of wild-type, *Skp2*$^{-/-}$, *p27*$^{-/-}$, and *Skp2*$^{-/-}$ *p27*$^{-/-}$ mice (Figures 2A–2L). As previously described, the nuclei of hepatocytes, renal tubule cells, and bronchiolar epithelial cells of *Skp2*$^{-/-}$ mice were substantially larger than those of the corresponding cells in wild-type littermates. Such nuclear enlargement was not apparent in the cells of *p27*$^{-/-}$ or *Skp2*$^{-/-}$ *p27*$^{-/-}$ mice. Flow cytometry also revealed that the DNA content of hepatocytes from *Skp2*$^{-/-}$ mice ranged from 2C to 16C, whereas that of most hepatocytes from wild-type or *p27*$^{-/-}$ animals was 2C or 4C (Figures 2M–2O). The percentage of polyploid cells in *Skp2*$^{-/-}$ *p27*$^{-/-}$ mice was greatly reduced compared with that in *Skp2*$^{-/-}$ mice, although the double mutant did exhibit a small increase in the number of 8C cells relative to that in wild-type animals (Figure 2P).

With the use of fluorescence microscopy, we also examined the nuclear size (as revealed by Hoechst 33258 staining) and centrosome number (as revealed by immunostaining with antibodies to pericentrin) of cultured mouse embryonic fibroblasts (MEFs) derived from the various mice. As with liver, kidney, and lung cells, MEFs derived from *Skp2*$^{-/-}$ mice exhibited a markedly enlarged nucleus, whereas the nuclear size of *Skp2*$^{-/-}$ *p27*$^{-/-}$ MEFs was similar to that of wild-type MEFs (Figures 2Q–2S). The number of centrosomes, which was increased in the *Skp2*$^{-/-}$ MEFs, also appeared normal in the *Skp2*$^{-/-}$ *p27*$^{-/-}$ cells (Figures 2T–2W). These observations indicate that the cellular phenotype of *Skp2*$^{-/-}$ mice is dependent on the presence of an intact p27 gene.

Mice lacking p27 manifest multiple organ hyperplasia, retinal dysplasia, and pituitary tumors (Fero et al., 1996; Kiyokawa et al., 1996; Nakayama et al., 1996). The most hyperplastic organs in these animals are the thymus, testis, ovary, adrenal medulla, and intermediate lobe of the pituitary gland. Histopathologic examination revealed that the adrenal medulla of *Skp2*$^{-/-}$ *p27*$^{-/-}$ mice is as hyperplastic as is that of *p27*$^{-/-}$ mice, whereas that of *Skp2*$^{-/-}$ mice appeared hypoplastic (Figures 3A–3D). Similarly, the intermediate lobe of the pituitary, a vestigial structure in adult humans, was hyperplastic in both

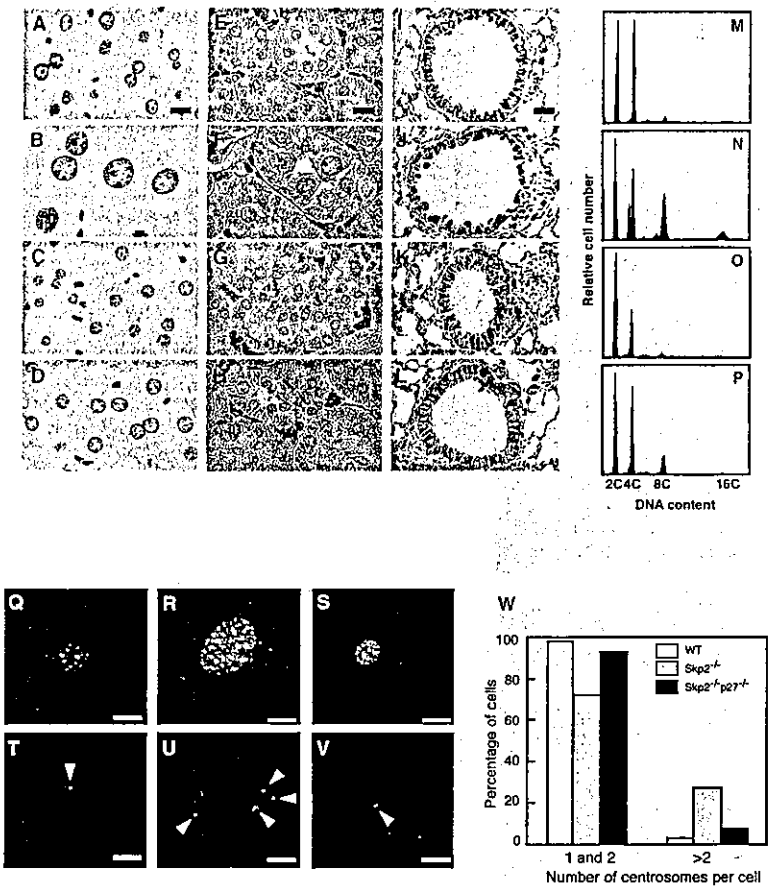

Figure 2. Absence of Nuclear Enlargement and Polyploidy in *Skp2*$^{-/-}$ *p27*$^{-/-}$ Mice

(A–L) Histological analysis of liver (A–D), renal tubules (E–H), and bronchioles (I–L) of adult wild-type (A, E, and I), *Skp2*$^{-/-}$ (B, F, and J), *p27*$^{-/-}$ (C, G, and K), and *Skp2*$^{-/-}$ *p27*$^{-/-}$ (D, H, and L) mice. Sections were stained with Feulgen solution (A–D) or with hematoxylin-eosin (E–L). Scale bars, 25 μm.

(M–P) Flow cytometric analysis of the DNA content of hepatocytes from wild-type (M), *Skp2*$^{-/-}$ (N), *p27*$^{-/-}$ (O), and *Skp2*$^{-/-}$ *p27*$^{-/-}$ (P) mice.

(Q–W) Normal nuclear size and centrosome number of *Skp2*$^{-/-}$ *p27*$^{-/-}$ cells. MEFs derived from wild-type (Q and T), *Skp2*$^{-/-}$ (R and U), and *Skp2*$^{-/-}$ *p27*$^{-/-}$ (S and V) embryos were stained either with both antibodies to β-tubulin and Hoechst 33258 (Q–S) or with antibodies to pericentrin alone (T–V). β-tubulin and pericentrin immune complexes are represented by red and green staining, respectively. Centrosomes are indicated by arrowheads. Blue staining represents Hoechst 33258 labeling of nuclear DNA. Scale bars, 10 μm. The percentages of MEFs either with one or two or with more than two centrosomes were determined by analysis of 400 cells per genotype (W).

p27$^{-/-}$ and *Skp2*$^{-/-}$ *p27*$^{-/-}$ mice (Figures 3E–3H). The intermediate lobe of these animals contained a large number of atypical cells; both *p27*$^{-/-}$ and *Skp2*$^{-/-}$ *p27*$^{-/-}$ mice were thus diagnosed with benign pituitary adenoma. Furthermore, histopathologic examination of the retina of *Skp2*$^{-/-}$ *p27*$^{-/-}$ mice revealed a marked disorganization of the cellular layers in the neural retina, similar to that apparent in *p27*$^{-/-}$ mice (Figures 3I–3L). These observations demonstrate that *Skp2*$^{-/-}$ *p27*$^{-/-}$ double mutant mice preserve the phenotypes of *p27*$^{-/-}$ mice. They therefore constitute genetic evidence in support of the notion that Skp2 is an upstream regulator of p27, although slight differences between *p27*$^{-/-}$ and *Skp2*$^{-/-}$ *p27*$^{-/-}$ mice may reflect other possible functions of Skp2.

Impaired Entry into M Phase in *Skp2*$^{-/-}$ Cells

We hypothesized that the nuclear enlargement, polyploidy, and centrosome overduplication apparent in *Skp2*$^{-/-}$ cells result from reentry of the cells into S phase without passage through M phase. To test this hypothesis, we orally administered the female hormone estriol, which transiently stimulates hepatocyte proliferation (Fujii et al., 1985), to adult wild-type, *Skp2*$^{-/-}$, *p27*$^{-/-}$, and *Skp2*$^{-/-}$ *p27*$^{-/-}$ mice. The giant cells observed in the liver of *Skp2*$^{-/-}$ mice were shown to have entered S phase by their incorporation of 5-bromo-2′-deoxyuridine (BrdU) that was injected intraperitoneally (Figures 4A and 4B). Monitoring of the time-dependent increase in the percentage of cells in S phase revealed no marked difference between wild-type and *Skp2*$^{-/-}$ mice (Figure 4C). Mitotic cells in the liver were evaluated by hematoxylin-eosin staining (data not shown) and immunostaining with antibodies to phosphorylated histone H3 (Figures 4D–4G), which is a marker for cells in M phase. In wild-type mice, cells containing phosphorylated histone H3 were apparent and peaked in number 5 days after estriol administration (Figure 4H). In contrast, no cells that reacted with the antibodies to the phosphorylated histone were detected at any time after estriol treatment in *Skp2*$^{-/-}$ mice. This lack of M phase induction in response to estriol appeared to be attributable to p27 accumulation, given that the liver of *Skp2*$^{-/-}$ *p27*$^{-/-}$ mice responded in a manner similar to that of the liver of wild-type mice (Figure 4G). These results thus suggested that *Skp2*$^{-/-}$ cells are able to enter S phase but not M phase, a characteristic of endoreplication, although a mitotic defect could also account for this abnormality. They also indicate that the inability of *Skp2*$^{-/-}$ cells to enter M phase is due to the abnormal accumulation of p27.

Impairment of Mitotic Entry Induced by a Reduction in Cdc2 Activity

In fission yeast, overexpression of the CKI Rum1 inhibits mitotic cyclin-Cdc2 activity and thereby prevents mitosis (Correa-Bordes and Nurse, 1995). Moreover, a high activity of the mitotic cyclin-Cdc2 complex prevents chromosome replication (Stern and Nurse, 1996). These observations led us to test the hypothesis that accumulation of the CKI p27 during G_2 phase inhibits mitotic cyclin-Cdc2 activity in mammalian *Skp2*$^{-/-}$ cells.

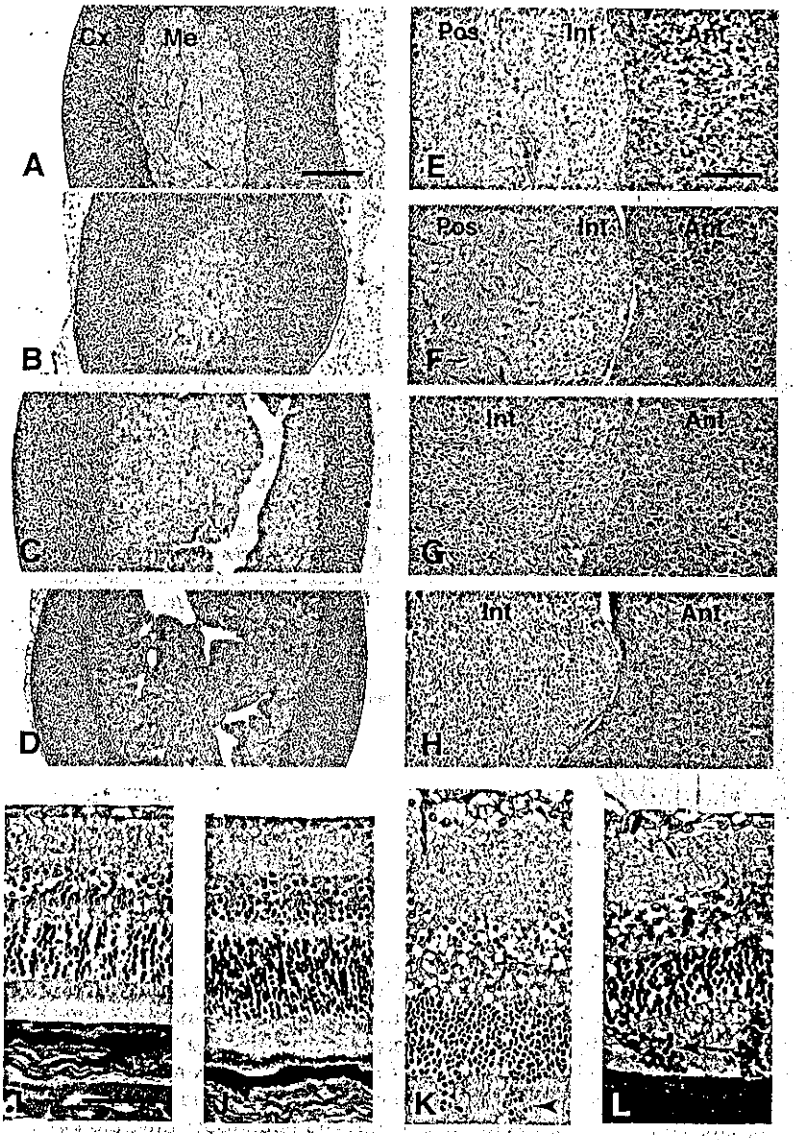

Figure 3. Organ Hyperplasia in *Skp2*$^{-/-}$ *p27*$^{-/-}$ Mice

Histological sections of the adrenal gland (A–D), pituitary gland (E–H), and retina (I–L) of wild-type (A, E, and I), *Skp2*$^{-/-}$ (B, F, and J), *p27*$^{-/-}$ (C, G, and K), and *Skp2*$^{-/-}$ *p27*$^{-/-}$ (D, H, and L) mice are shown. The paraffin-embedded sections were stained with hematoxylin-eosin. Abbreviations: Cx, cortex; Me, medulla; Ant, anterior lobe; Int, intermediate lobe; Pos, posterior lobe. Arrowheads in (K) and (L) indicate the outer granular layer invading the layer of rods and cones beyond the outer limiting membrane of the retina. Scale bars: 400 μm (A–D), 100 μm (E–H), and 25 μm (I–L).

We compared the abundance (Figure 5A) and kinase activities (Figure 5B) of various cell cycle regulators in MEFs derived from wild-type, *Skp2*$^{-/-}$, *p27*$^{-/-}$, and *Skp2*$^{-/-}$ *p27*$^{-/-}$ mice. There were no marked differences in the amounts of cyclin A, cyclin B, Cdk2, or Cdc2 or in the kinase activity associated with Cdk2 among the four types of cells. In contrast to lymphocytes, which express p27 but not p57 (Nagahama et al., 2001), and in which the loss of p27 results in a marked increase in the kinase activity of Cdk2 (Nakayama et al., 1996), *p27*$^{-/-}$ MEFs did not exhibit an increase in such activity, probably because of the presence of p57. Cyclin A-, cyclin B-, or Cdc2-associated kinase activity was substantially reduced in *Skp2*$^{-/-}$ cells compared with that in MEFs of the other three genotypes, however. The observation that *Skp2*$^{-/-}$ *p27*$^{-/-}$ MEFs differed from *Skp2*$^{-/-}$ cells in this regard suggests that accumulation of p27 is responsible for the low kinase activity of cyclin A-Cdc2 or cyclin B-Cdc2 in *Skp2*$^{-/-}$ cells. Cyclin E-associated kinase activity was not increased, even though the abundance of cyclin E was increased, in the *Skp2*$^{-/-}$ cells, suggesting that the accumulated p27 antagonized the kinase activity. Consistent with this notion, the activity of cyclin E-associated kinase activity was increased in *Skp2*$^{-/-}$ *p27*$^{-/-}$ MEFs.

We found that p27 associated with Cdc2, although to only a small extent, in wild-type MEFs (Figure 5C). The amount of Cdc2 bound to endogenous p27 was markedly increased in *Skp2*$^{-/-}$ cells, however. The phosphorylation status of tyrosine-15 and threonine-161 of Cdc2 was similar among the four genotypes of MEFs (Supplemental Figure S1 at http://www.developmentalcell.com/cgi/content/full/6/5/661/DC1), excluding the possibility that the loss of Skp2 or accumulation of p27 affects other molecules that regulate Cdc2 activity directly. The amount of Cdk2 associated with p27 was also increased in *Skp2*$^{-/-}$ cells (Figure 5C). In contrast, the amount of Cdk4 associated with p27 was not affected by the loss of Skp2, which might be explained if the amount of Cdk4 is limited and most of it is bound to p27 even in wild-type cells; the excess p27 that overflows from the Cdk4-bound pool would then be available to bind to Cdk2 or

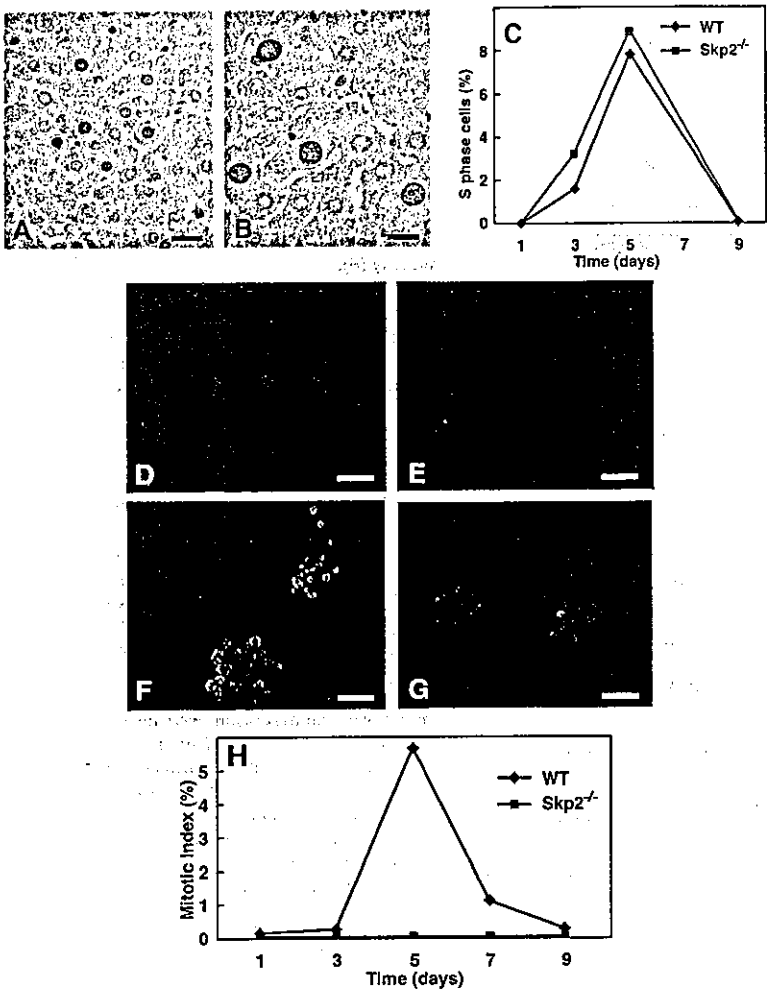

Figure 4. Defective Entry into M Phase of Hepatocytes Exposed to Mitogenic Stimulation in Adult *Skp2*$^{-/-}$ Mice

Adult mice were subjected to a single oral administration of estriol and daily intraperitoneal injection of BrdU. They were killed at various times after estriol administration and sections of the liver were processed for immunostaining.

(A and B) Liver sections prepared from wild-type (A) and *Skp2*$^{-/-}$ (B) mice 5 days after administration of estriol were subjected to immunostaining with antibodies to BrdU (brown).

(C) The percentage of liver cells that stained with the antibodies to BrdU was determined for wild-type and *Skp2*$^{-/-}$ mice at the indicated times after administration of estriol.

(D–G) Liver sections prepared from wild-type (D), *Skp2*$^{-/-}$ (E), *p27*$^{-/-}$ (F), and *Skp2*$^{-/-}$ *p27*$^{-/-}$ (G) mice 5 days after estriol administration were stained with antibodies to phosphorylated histone H3 (red) and Hoechst 33258 (blue).

(H) The percentage of liver cells that stained with the antibodies to phosphorylated histone H3 (mitotic index) was determined for wild-type and *Skp2*$^{-/-}$ mice at the indicated times after administration of estriol.

Data in (C) and (H) are from representative animals. Scale bars: 50 μm (A and B) and 25 μm (D–G).

Cdc2 in *Skp2*$^{-/-}$ MEFs. Immunodepletion of p27 also reduced the amounts of Cdc2 and Cdk2 in *Skp2*$^{-/-}$ cell lysates (data now shown), confirming that a substantial proportion of Cdc2 and Cdk2 is bound to endogenous p27. We also found that FLAG epitope-tagged exogenous p27 interacted with endogenous cyclin A, cyclin B, Cdk2, and Cdc2 as well as inhibited the associated kinase activities in COS-7 cells (Figure 5D). Mass spectrometric analysis of immunoprecipitates prepared from HEK293T cells expressing FLAG-tagged p27 with antibodies to FLAG showed that p27 is complexed with cyclin A2, cyclin B1, cyclin B2, cyclin E1, cyclin E2, Cdc2, Cdk2, Cdk4, and Cdk5 (data not shown).

We next examined whether the observed decrease in the kinase activity of Cdc2 is sufficient to explain the overreplication phenotype of *Skp2*$^{-/-}$ cells. We first treated wild-type MEFs with a potent Cdc2 inhibitor, butyrolactone I (Kitagawa et al., 1993). Exposure of the wild-type MEFs to butyrolactone I resulted in nuclear enlargement and centrosome multiplication (Figures 6A and 6B), characteristics similar to those of *Skp2*$^{-/-}$ MEFs. Flow cytometric analysis revealed that the DNA content of the butyrolactone I-treated cells increased in multiples of 2C (Figure 6C), a characteristic of endoreplication, rather than in a continuous manner, as would be consistent with DNA rereplication. Cell size was also increased by treatment with butyrolactone I (Figure 6D). Given that this compound may affect other types of Cdk, we also examined FT210 cells, which express a temperature-sensitive mutant of Cdc2 (Th'ng et al., 1990). FM210 cells cultured at the restrictive temperature (39°C) exhibited huge nuclei and multiple centrosomes (Figure 6H); neither FM210 cells cultured at the permissive temperature (32°C) (Figure 6G) nor the parental cell line, FM3A, cultured at either temperature (Figures 6E and 6F) exhibited this phenotype. Flow cytometric analysis revealed that FT210 cells cultured at the restrictive temperature, but not those cultured at the permissive temperature, appeared to be arrested at the G_2-M boundary (Figure 6I) with an increase in cell size (Figure 6J). These data thus indicate that a reduction in the kinase activity of Cdc2 results in G_2-M arrest associated with nuclear enlargement and centrosome overduplication in mammalian cells. In *Skp2*$^{-/-}$ mice, the accumulation of p27 due to the lack of its ubiquitylation-mediated proteolysis likely results in such a decrease in Cdc2 activity.

Accumulation of Cyclin E in *Skp2*$^{-/-}$ *p27*$^{-/-}$ Mice

Given that p27 is an inhibitor of the kinase activity of cyclin E-Cdk2 and that the phosphorylation of cyclin E that triggers its degradation is thought to be mediated,

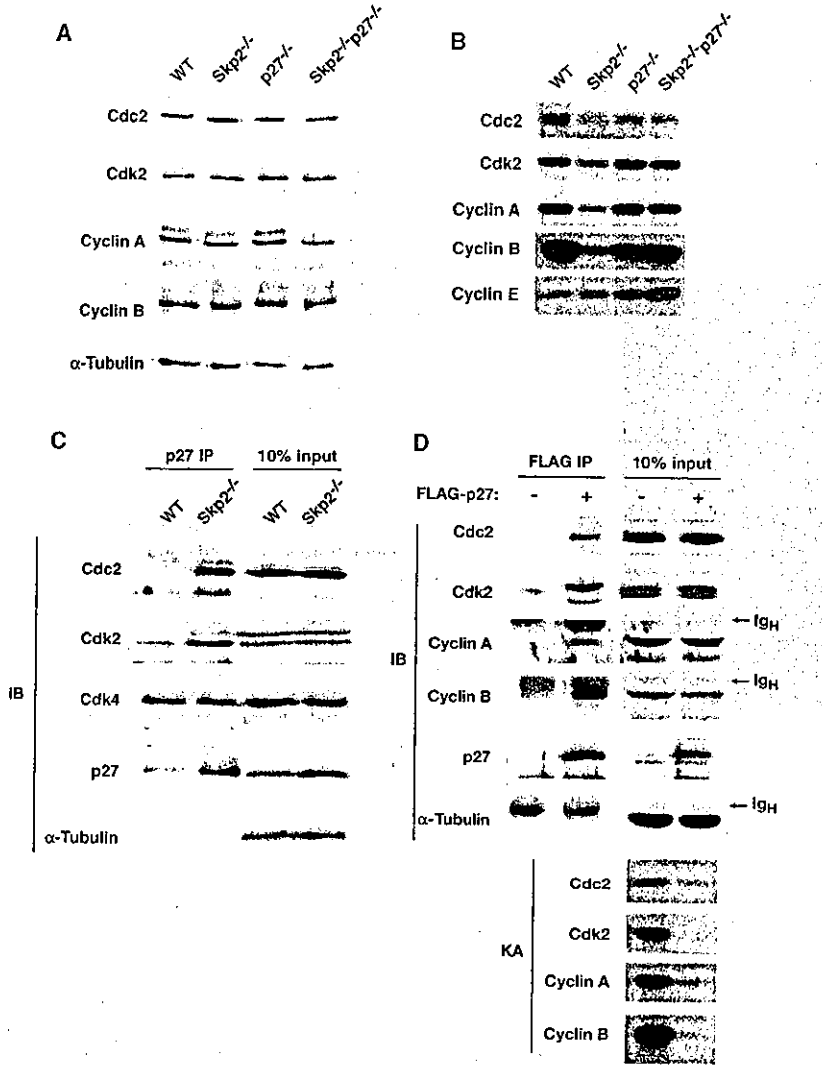

Figure 5. Reduced Cdc2-, Cyclin A-, or Cyclin B-Associated Kinase Activity in *Skp2*$^{-/-}$ Cells and Interaction of p27 with Cdc2, Cdk2, Cyclin A, and Cyclin B

(A and B) Lysates of MEFs from wild-type, *Skp2*$^{-/-}$, *p27*$^{-/-}$, and *Skp2*$^{-/-}$ *p27*$^{-/-}$ mice were subjected either to immunoblot analysis with antibodies to the indicated proteins (A) or to in vitro assays of Cdc2-, Cdk2-, cyclin A-, cyclin B-, or cyclin E-associated kinase activity (B).

(C) Lysates of MEFs from wild-type and *Skp2*$^{-/-}$ mice were subjected to immunoprecipitation (IP) with antibodies to p27, and the resulting precipitates were subjected to immunoblot (IB) analysis with antibodies to the indicated proteins (left panels). A portion (10%) of the input lysates was also subjected directly to immunoblot analysis with the same antibodies (right panels).

(D) COS-7 cells were transfected with an expression vector for FLAG-tagged p27 (or with the empty vector) and with a vector for CD19, and CD19-expressing cells were then isolated with the use of magnetic beads conjugated with antibodies to CD19. Lysates of the CD19-positive cells were subjected to immunoprecipitation with antibodies to FLAG, and the resulting precipitates were subjected to immunoblot analysis with antibodies to the indicated proteins (left panels). Portions (10%) of the input lysates were also subjected directly to immunoblot analysis with the same antibodies (upper right panels) and to in vitro assays of kinase activity (KA) associated with the indicated proteins (lower right panels). Ig_H, immunoglobulin heavy chain.

at least in part, by associated Cdk2, it was possible that the accumulation of cyclin E in the cells of *Skp2*$^{-/-}$ mice was an indirect consequence of p27 accumulation. To investigate this possibility, we examined the amount of cyclin E in MEFs, thymus, testis, and liver of *Skp2*$^{-/-}$ *p27*$^{-/-}$ mice. The abundance of cyclin E in these cells and tissues of the double mutant, however, was markedly greater than that in their wild-type counterparts and similar to that for *Skp2*$^{-/-}$ mice (Figure 7A), suggesting that the accumulation of cyclin E in *Skp2*$^{-/-}$ cells is not dependent on p27 accumulation. The amount of phosphorylated cyclin E in MEFs was similar for the four genotypes (Supplemental Figure S2A at http://www.developmentalcell.com/cgi/content/full/6/5/661/DC1), suggesting that the cyclin E that accumulates in *Skp2*$^{-/-}$ mice is the nonphosphorylated form. The p27-related CKIs p21 and p57, both of which are also targets of Skp2-mediated ubiquitylation (Bornstein et al., 2003; Kamura et al., 2003), were also examined for their binding to cyclin E in wild-type, *Skp2*$^{-/-}$, *p27*$^{-/-}$, and *Skp2*$^{-/-}$ *p27*$^{-/-}$ MEFs. Like p27, more p21 was associated with cyclin E in *Skp2*$^{-/-}$ MEFs than in wild-type MEFs (Supplemental Figure S2B); the increase in the amount of p21 bound to cyclin E was also observed in *Skp2*$^{-/-}$ *p27*$^{-/-}$ MEFs. Association of p57 with cyclin E was not detected in MEFs of any of the four genotypes (data not shown). We therefore are not able to exclude completely the possibility that accumulation of p21 or of other proteins results in inhibition of cyclin E-associated kinase activity and thereby stabilizes cyclin E by blocking its phosphorylation. However, such a possibility seems unlikely because cyclin E-associated kinase activity was not reduced in *Skp2*$^{-/-}$ MEFs (Figure 5B).

We also measured the rate of cyclin E degradation by treatment of MEFs with the protein synthesis inhibitor cycloheximide. In asynchronously cycling cells, cyclin E appeared to be more stable in *Skp2*$^{-/-}$ and *Skp2*$^{-/-}$ *p27*$^{-/-}$ cells than in wild-type or *p27*$^{-/-}$ cells (Figures 7B and 7C). This result was verified by pulse-chase experiments (Supplemental Figure S3). Furthermore, cyclin E was rapidly degraded after the release of wild-type and *p27*$^{-/-}$ MEFs from S phase arrest induced by aphidicolin treatment (Figures 7D and 7E); in contrast, the degradation of cyclin E after release from aphidicolin block was markedly delayed in *Skp2*$^{-/-}$ and *Skp2*$^{-/-}$ *p27*$^{-/-}$ MEFs. In addition, our previous biochemical

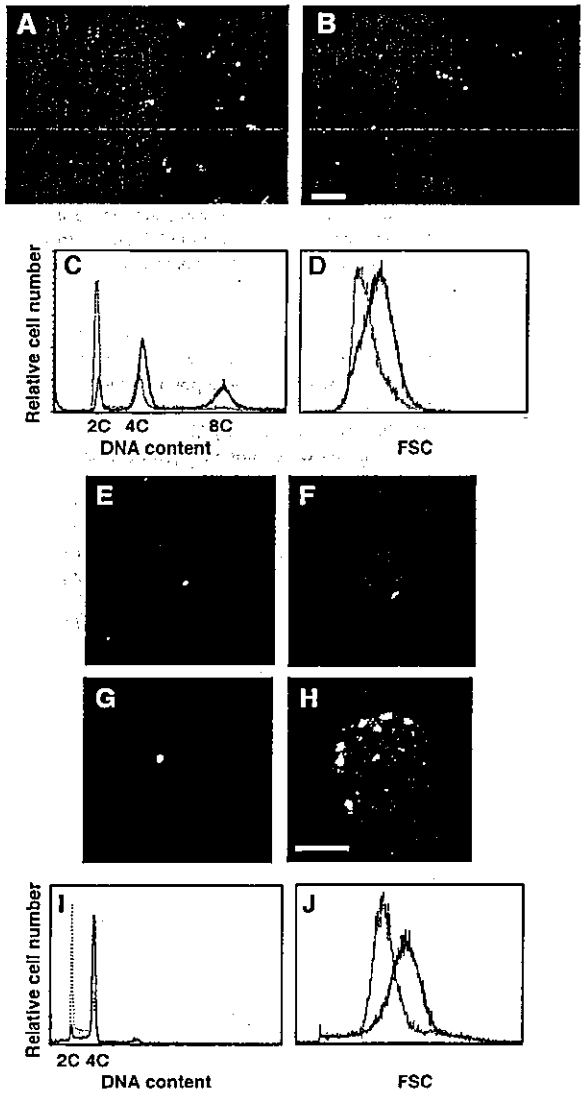

Figure 6. Induction of Nuclear Enlargement by Inhibition of the Kinase Activity of Cdc2

(A–D) Wild-type MEFs were incubated for 72 hr with dimethyl sulfoxide (vehicle control) (A) or with 80 μM butyrolactone I (B), after which they were subjected to immunostaining with antibodies to pericentrin (green) or to β-tubulin (red). Blue staining represents Hoechst 33258 labeling of nuclear DNA. Scale bar, 20 μm. The DNA content (C) and forward light scatter (FSC) (D) of the cells cultured in the absence (dotted lines) or presence (solid lines) of butyrolactone I were also measured by flow cytometry.

(E–J) FT210 cells (G and H), which express a temperature-sensitive mutant of Cdc2, and the parental FM3A cells (E and F) were cultured at 32°C (permissive temperature) (E and G) or 39°C (restrictive temperature) (F and H), after which they were subjected to immunostaining with antibodies to pericentrin (green) and to staining of DNA with propidium iodide (red). The images were taken by laser-scanning confocal microscopy. Scale bar, 10 μm. FT210 cells cultured at the permissive (dotted lines) or restrictive (solid lines) temperature were also subjected to flow cytometric analysis of DNA content (I) or forward light scatter (J).

studies indicated that Skp2 specifically interacts with cyclin E and thereby promotes its ubiquitylation and degradation both in vivo and in vitro (Nakayama et al., 2000). Collectively, these findings suggest that free cyclin E is a candidate substrate of SCF^{Skp2}, and that accumulation of cyclin E alone is not the cause of the cellular abnormalities of *Skp2*$^{-/-}$ mice.

Discussion

p27 Is a Major Physiological Target of SCF^{Skp2}

Protein degradation by the ubiquitin-proteasome pathway plays a fundamental role in determining the abundance of important regulatory molecules. The E3 ubiquitin ligases are thought to determine the substrate specificity of this pathway, and many diverse E3 molecules are therefore thought to exist, although it does not appear to be unusual that several proteins serve as substrates for a given ubiquitin ligase. Skp2, the substrate-recognizing component of an SCF ubiquitin ligase, has thus been shown to recognize p27 (Carrano et al., 1999; Sutterluty et al., 1999; Tsvetkov et al., 1999; Nakayama et al., 2000), the p27-related CKIs p21 (Yu et al., 1998; Bornstein et al., 2003) and p57 (Kamura et al., 2003), cyclin A (Nakayama et al., 2000), cyclin D1 (Yu et al., 1998), free cyclin E (Nakayama et al., 2000), E2F-1 (Marti et al., 1999), p130 (Tedesco et al., 2002; Bhattacharya et al., 2003), ORC1 (Mendez et al., 2002), Cdt1 (Li et al., 2003), Cdk9 (Kiernan et al., 2001), c-Myc (Kim et al., 2003; von der Lehr et al., 2003), and B-Myb (Charrasse et al., 2000). Of these proteins, cyclin A, cyclin D1, E2F-1, and Cdt1 do not accumulate in *Skp2*$^{-/-}$ cells (Nakayama et al., 2000) (our unpublished data), suggesting either that they are not bona fide substrates of Skp2 or that there is redundancy that allows for their ubiquitylation in the absence of Skp2.

Most of the cellular abnormalities apparent in *Skp2*$^{-/-}$ mice are not evident in *Skp2*$^{-/-}$ *p27*$^{-/-}$ double mutant mice. This observation constitutes genetic evidence that the cellular phenotype of nuclear enlargement with polyploidy and overduplication of centrosomes in *Skp2*$^{-/-}$ mice results from the deregulated expression of p27 during the cell cycle, and that p27 is likely the main target of the SCF^{Skp2} ubiquitin ligase. However, the observation that the phenotype of *Skp2*$^{-/-}$ *p27*$^{-/-}$ mice is not completely identical to that of *p27*$^{-/-}$ mice suggests the existence of additional target proteins for Skp2-mediated ubiquitylation.

Role of Skp2 in Prevention of p27 Accumulation during S and G_2 Phases

The concentration of p27 is relatively high in quiescent (G_0) cells, decreases on entry of cells into the cell cycle, and is controlled predominantly by the rate of p27 degradation (Pagano et al., 1995; Shirane et al., 1999) as well as by translational regulation (Hengst and Reed, 1996). This degradation has been thought to require Skp2, which binds to p27 when the latter is phosphorylated on Thr^{187} by the cyclin E–Cdk2 complex (Sheaff et al., 1997; Vlach et al., 1997; Carrano et al., 1999; Montagnoli et al., 1999; Sutterluty et al., 1999; Tsvetkov et al., 1999). The primary function of SCF^{Skp2} might therefore be to render quiescent cells competent to reenter the cell cycle by mediating the degradation of p27. However, there are several inconsistencies with this notion. Skp2 and cyclin E are not expressed until the G_1-S transition of the cell cycle, unequivocally later than the onset of

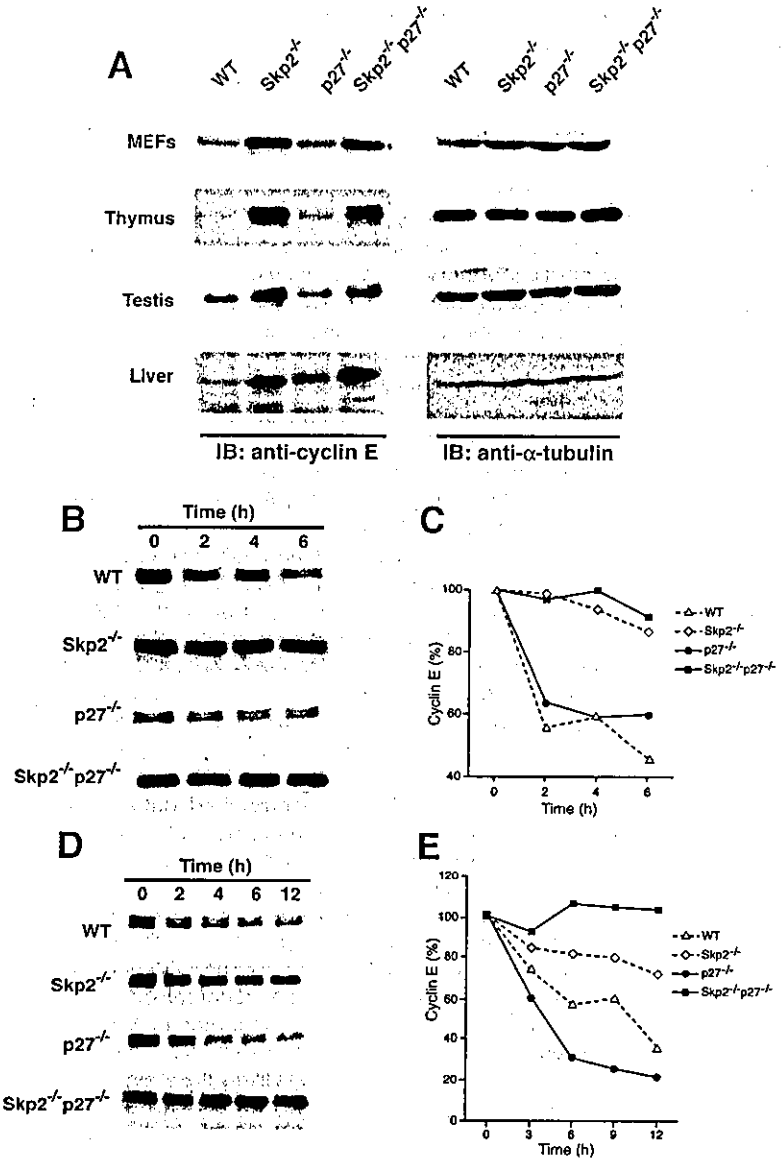

Figure 7. Impaired Degradation of Cyclin E in *Skp2*$^{-/-}$ Mice Is Independent of p27

(A) Immunoblot analysis of cyclin E (left panels) and α-tubulin (control; right panels) in lysates prepared from MEFs, thymus, testis, and liver of wild-type, *Skp2*$^{-/-}$, *p27*$^{-/-}$, and *Skp2*$^{-/-}$ *p27*$^{-/-}$ mice.

(B) Proliferating wild-type, *Skp2*$^{-/-}$, *p27*$^{-/-}$, or *Skp2*$^{-/-}$ *p27*$^{-/-}$ MEFs were incubated in the presence of cycloheximide (50 μg/ml) for the indicated times, after which cell lysates were subjected to immunoblot analysis with antibodies to cyclin E.

(C) The band intensities in (B) were quantitated by image analysis and expressed as a percentage of the corresponding value for time zero.

(D) Wild-type, *Skp2*$^{-/-}$, *p27*$^{-/-}$, or *Skp2*$^{-/-}$ *p27*$^{-/-}$ MEFs were synchronized at S phase by treatment with aphidicolin (1 μg/ml) for 15 hr and then released into aphidicolin-free medium for the indicated times, after which cell lysates were prepared and subjected to immunoblot analysis with antibodies to cyclin E.

(E) The band intensities in (D) were quantitated and expressed as described in (C).

p27 degradation apparent at mid-G_1 phase (Hara et al., 2001). Moreover, p27 is exported from the nucleus to the cytoplasm at G_0-G_1 (Tomoda et al., 1999; Rodier et al., 2001; Ishida et al., 2002; Connor et al., 2003), whereas Skp2 is restricted to the nucleus (Miura et al., 1999). The discrepancies between the temporal and spatial patterns of p27 expression and those of Skp2 expression suggest the existence of a Skp2-independent pathway for the degradation of p27. Indeed, the downregulation of p27 at the G_0-G_1 transition occurs normally in *Skp2*$^{-/-}$ cells and is sensitive to proteasome inhibitors (Hara et al., 2001). Biochemical analysis of crude extracts of *Skp2*$^{-/-}$ cells revealed the presence in the cytoplasmic fraction of an Skp2-independent E3 activity that mediates the ubiquitylation of p27 (Hara et al., 2001). This ubiquitylation was not dependent on the phosphorylation of p27 on Thr^{187}, which is a prerequisite for Skp2-mediated ubiquitylation. These data indicate that p27 is degraded at the G_0-G_1 transition by a proteasome-dependent, but Skp2-independent, mechanism.

In contrast, the degradation of p27 during S and G_2 phases is impaired in *Skp2*$^{-/-}$ mice, suggesting that the primary function of Skp2 is to prevent both the accumulation of p27 during S and G_2 phases and the consequent inhibition of mitotic cyclin-Cdc2 activity. Consistent with this idea, experimental inhibition of the kinase activity of Cdc2 in budding yeast, fission yeast, and *Drosophila* forces cells that are normally mitotic to become endoreplicative (Edgar and Orr-Weaver, 2001). In the present study, we show that this is also the case, at least in part, in mammals. Cell cycle synchronization of *Skp2*$^{-/-}$ MEFs also revealed a delay at the G_2-M boundary in comparison with wild-type and *Skp2*$^{-/-}$ *p27*$^{-/-}$ cells (Supplemental Figure S4 at http://www.developmentalcell.com/cgi/content/full/6/5/661/DC1). These data suggest that inactivation of Cdc2 by p27 that accumulates as a result of the lack of Skp2 leads to G_2-M block, although the detailed mechanism of this phenomenon remains to be determined. We thus propose that the major target of p27 at G_1 phase is Cdk2, and that at G_2 phase it may

be Cdc2; Skp2 seems to be important for the regulation of the latter.

Endoreplication of Hepatocytes Induced by Deregulation of p27 Degradation

Polyploidy is apparent in certain tissues of *Skp2*$^{-/-}$ mice including the liver. Maintenance of genome ploidy is a fundamental aspect of cell division. Three possible mechanisms might render cells polyploid. (1) Failure of mitosis. Cells enter mitosis normally but anaphase fails to occur, resulting in the subsequent entry of the cells into interphase with a doubled DNA content. (2) Endoreplication. Cells replicate their genomes in S phase, bypass mitosis, and double their DNA content again in the next S phase. (3) DNA rereplication. Cells arrest in S phase and reinitiate DNA replication continuously. We adopted two criteria to determine which of these three mechanisms gives rise to the polyploidy of *Skp2*$^{-/-}$ hepatocytes. First, we examined whether cells entered mitosis. Immunofluorescence analysis with antibodies to phosphorylated histone H3, a marker of early mitosis, revealed that the number of mitotic cells is reduced in the liver of *Skp2*$^{-/-}$ mice, suggesting that failure of mitosis is not likely responsible for the polyploidy in these animals. Second, we measured the DNA content of *Skp2*$^{-/-}$ hepatocytes after mitogenic stimulation in order to determine whether the increase in DNA content occurred in a stepwise manner. The DNA content of *Skp2*$^{-/-}$ cells was shown to increase in multiples of 2C, a characteristic of endoreplication, rather than in a continuous manner, as would be consistent with DNA rereplication (data not shown). Similar results were also obtained after partial hepatectomy in *Skp2*$^{-/-}$ mice (Minamishima et al., 2002). We thus conclude that the polyploidy of *Skp2*$^{-/-}$ hepatocytes is likely attributable to endoreplication, although the possibility of a mitotic defect cannot be formally ruled out.

The regulation of Cdk activity during endoreplication in mammalian cells, with the exception of megakaryocytes and trophoblasts, is poorly understood (Edgar and Orr-Weaver, 2001). Consistent with the association of Skp2 with Cul1 in the SCF ubiquitin ligase complex, the phenotype of trophoblasts of *Cul1*$^{-/-}$ embryos is similar to that of *Skp2*$^{-/-}$ cells (Dealy et al., 1999; Wang et al., 1999). Unlike most cells, trophoblasts undergo multiple rounds of DNA synthesis without an intervening mitosis, resulting in the formation of giant nuclei (Zybina and Zybina, 1996). The lack of Cul1 or Skp2 appears to augment this process, and our present data indicate that the accumulation of p27 may play an important role in its induction. The abundance of cyclin E remains high and that of cyclin B is reduced in a differentiating trophoblast cell line, and p57, which is structurally and functionally similar to p27, is upregulated during S phase in these cells (Hattori et al., 2000). These characteristics resemble those of *Skp2*$^{-/-}$ cells. However, ectopic expression of a form of p57 with a mutation that stabilizes the protein blocks S phase entry in the trophoblast cell line. The gradual increase in the abundance of p27 in *Skp2*$^{-/-}$ cells may give rise to a window in which p27 inhibits mitosis but not entry into S phase, whereas forced expression of p57 at high levels may block S phase entry immediately.

A fission yeast mutant that lacks the F box protein Pop1, which targets the CKI Rum1 for degradation, also exhibits endoreplication and consequent polyploidy (Kominami and Toda, 1997). Rum1 accumulates to high levels in this mutant. Maintenance of ploidy in fission yeast is controlled by a complex of Cdc2 with the mitotic cyclin Cdc13. Inhibition of the kinase activity of Cdc2-Cdc13 as a result of the increased expression of Rum1 in the *pop1* mutant thus likely leads to polyploidy by promoting the bypass of M phase before the next S phase. A mitotic cyclin-Cdk complex in budding yeast prevents endoreplication through multiple overlapping mechanisms, including phosphorylation of the origin recognition complex (ORC), downregulation of Cdc6 activity, and exclusion from the nucleus of the Mcm2-7 complex (Nguyen et al., 2001). Given the similarities in the phenotypes of the fission yeast *pop1* mutant and mouse *Skp2*$^{-/-}$ cells, the accumulation of p27 in *Skp2*$^{-/-}$ cells may functionally correspond to that of Rum1 in the *pop1* mutant. The prevention of endoreplication through degradation of a CKI mediated by an SCF ubiquitin ligase thus appears to be a mechanism that has been well conserved from yeast to mammals.

Free Cyclin E as a Potential Substrate of SCF^{Skp2}

The marked accumulation of cyclin E in the absence of the antagonizing action of p27 in *Skp2*$^{-/-}$ *p27*$^{-/-}$ mice might have been expected either to compromise tissue organization in the developing embryo, and thereby to result in early embryonic death, or to lead to a high incidence of carcinogenesis. The apparent absence of such outcomes suggests that the deregulated expression of cyclin E might not be a direct cause of carcinogenesis, even though altered expression of cyclin E is apparent in many human cancers. The cyclin E that accumulates in *Skp2*$^{-/-}$ mice, however, appears to be the free form of the protein (Nakayama et al., 2000), not that complexed with Cdk2, and therefore does not contribute to the kinase activity of Cdk2. The nature of the interaction between the pool of free cyclin E and the cyclin E-Cdk2 complex is unclear, but our present data suggest that a simple increase in the abundance of free cyclin E does not directly result in the activation of Cdk2. Another possible interpretation of our data is that the increase in the pool of free cyclin E in *Skp2*$^{-/-}$ cells results in an increase in the activity of the cyclin E-Cdk2 complex, but that this effect is antagonized by the accumulated p27.

Our data do not necessarily imply that SCF^{Skp2} is the main mediator of cyclin E turnover. Rather, the mechanisms for the degradation of cyclin E appear complex. The Skp2-Cul1 complex and Cul3 interact with the free, nonphosphorylated form of cyclin E (Dealy et al., 1999; Singer et al., 1999; Wang et al., 1999; Nakayama et al., 2000), thereby mediating its ubiquitylation-dependent proteolysis. In parallel with these pathways, SCF^{Fbw7} is thought to target phosphorylated cyclin E complexed with Cdk2 (Clurman et al., 1996; Won and Reed, 1996; Koepp et al., 2001; Moberg et al., 2001; Strohmaier et al., 2001). However, mice that lack Fbw7, which die in utero during embryogenesis, show neither accumulation of cyclin E nor an increase in Cdk2 activity (Tsunematsu et al., 2004), whereas *Skp2*$^{-/-}$ mice manifest marked

accumulation of cyclin E in the nucleus. Thus, Fbw7 appears to be dispensable for cyclin E degradation, at least until mid-embryogenesis. In contrast, depletion of Fbw7 by RNA interference results in the accumulation of cyclin E in cultured cells (Koepp et al., 2001) (our unpublished observations), suggesting that Fbw7 might be required for cyclin E turnover in adult tissues. These data render unlikely, however, the possibility that the loss of Skp2 might stabilize other proteins that impair the Fbw7-dependent pathway of protein degradation and are thereby responsible for the accumulation of cyclin E.

Given that p27 accumulates to a high level in *Skp2*$^{-/-}$ cells, it is possible that autophosphorylation of cyclin E complexed with Cdk2 is inhibited by this CKI, resulting in stabilization of cyclin E. The accumulation of cyclin E might thus be secondary to the increase in the abundance of p27. Our present data, however, have shown that cyclin E degradation is also impaired in *Skp2*$^{-/-}$ *p27*$^{-/-}$ mice, providing genetic evidence that the altered expression of cyclin E in *Skp2*$^{-/-}$ cells is independent of p27 accumulation. We have previously shown that Skp2 interacts with free cyclin E and promotes its ubiquitylation both in vitro and in vivo, and that cyclin E degradation is impaired, resulting in loss of periodicity of cyclin E expression, in *Skp2*$^{-/-}$ cells (Nakayama et al., 2000). These biochemical observations are therefore consistent with the genetic evidence that Skp2 directly targets cyclin E. It remains possible that the accumulation of CKIs such as p21, p107, and p130 in *Skp2*$^{-/-}$ mice contributes to the stabilization of cyclin E, although our observation that the kinase activity of Cdk2 is unchanged in *Skp2*$^{-/-}$ cells suggests against this possibility.

Experimental Procedures

Mice

Both Skp2-deficient mice and p27-deficient mice were generated in our laboratory (Nakayama et al., 1996, 2000). We have developed polymerase chain reaction-based protocols (details available on request) to identify wild-type and disrupted alleles of *Skp2* and *p27*.

Histological and Immunofluorescence Analyses

Histological analysis and immunofluorescence analysis of centrosomes and microtubules were performed as described (Nakayama et al., 2000).

Preparation of MEFs

Primary MEFs were isolated from embryos on embryonic day 13.5 and cultured as previously described (Nakayama et al., 1996). In asynchronous culture, there was no substantial difference in cell cycle profiles among wild-type, *Skp2*$^{-/-}$, *p27*$^{-/-}$, and *Skp2*$^{-/-}$ *p27*$^{-/-}$ MEFs (Supplemental Figure S4A at http://www.developmentalcell.com/cgi/content/full/6/5/661/DC1).

Flow Cytometry

Flow cytometric analysis of hepatocytes and MEFs was performed as described previously (Nakayama et al., 1996, 2000).

Immunoblot Analysis

Transfection, immunoprecipitation, and immunoblot analysis were performed as previously described (Hatakeyama et al., 1999; Kitagawa et al., 1999). Antibodies used in this study include those to cyclin A (H-432, Santa Cruz Biotechnology), cyclin B (GNS-1, PharMingen), cyclin E (M-20, Santa Cruz Biotechnology), Cdk2 (M2, Santa Cruz Biotechnology), Cdc2 (17, Santa Cruz Biotechnology), p27 (57, Transduction Laboratories), or α-tubulin (TU-01, Zymed), each at a concentration of 0.2 μg/ml.

In some experiments, subconfluent COS-7 cells grown in four 100 mm dishes were transfected with 5 μg of pcDNA3 or pcDNA-FLAG-p27 and with 2 μg of pCD19 (Tedder and Isaacs, 1989) per dish with the use of the FuGENE6 reagent (Roche Molecular Biochemicals). Twenty-four hours after transfection, the CD19-expressing cells were collected with antibodies to CD19 attached to magnetic beads (Dynal Biotech) and were used for immune-complex kinase assays and immunoprecipitation.

Immune-Complex Kinase Assays

Kinase activity associated with Cdk2, Cdc2, or cyclins A, B, or E was measured with an immune-complex kinase assay as described (Nakayama et al., 1996).

Mitogenic Stimulation of Mouse Hepatocytes by Oral Administration of Estriol

Male mice at 8 weeks of age were subjected to oral administration of 0.4 mg of estriol (Wako) per gram of body mass. They were also subjected to daily intraperitoneal injection of BrdU (100 μg/g) (Sigma). Colchicine (1 μg/g) (Wako) was injected intraperitoneally 6 hr before killing. Sections of the liver were stained with hematoxylin-eosin or were subjected to immunostaining with rabbit polyclonal antibodies to phosphorylated histone H3 (Upstate Biotechnology) followed by Cy3-conjugated goat antibodies to rabbit immunoglobulin G (Chemicon). For detection of BrdU, sections were incubated with a rat monoclonal antibody to BrdU (Harlan Sera-Lab) at a dilution of 1:200 followed by biotinylated secondary antibodies; immune complexes were visualized with the use of a streptavidin-biotin-peroxidase detection kit (Vector) and diaminobenzidine (Wako).

Acknowledgments

We thank M. Fujita for helpful discussions, R. Tsunematsu, M. Matsumoto, T. Hara, Y. Yamada, K. Shimoharada, S. Matsushita, N. Nishimura, R. Yasukochi, A. Ito, Y. Ono, and other laboratory members for technical assistance, and M. Kimura and C. Sugita for help in preparation of the manuscript. This work was supported in part by a research grant from the Human Frontier Science Program.

Received: September 25, 2003
Revised: March 19, 2004
Accepted: March 24, 2004
Published: May 10, 2004

References

Bhattacharya, S., Garriga, J., Calbo, J., Yong, T., Haines, D.S., and Grana, X. (2003). SKP2 associates with p130 and accelerates p130 ubiquitylation and degradation in human cells. Oncogene *22*, 2443–2451.

Bornstein, G., Bloom, J., Sitry-Shevah, D., Nakayama, K., Pagano, M., and Hershko, A. (2003). Role of the SCF^{Skp2} ubiquitin ligase in the degradation of p21^{Cip1} in S phase. J. Biol. Chem. *278*, 25752–25757.

Carrano, A.C., Eytan, E., Hershko, A., and Pagano, M. (1999). SKP2 is required for ubiquitin-mediated degradation of the CDK inhibitor p27. Nat. Cell Biol. *1*, 193–199.

Charrasse, S., Carena, I., Brondani, V., Klempnauer, K.H., and Ferrari, S. (2000). Degradation of B-Myb by ubiquitin-mediated proteolysis: involvement of the Cdc34-SCF(p45^{Skp2}) pathway. Oncogene *19*, 2986–2995.

Clurman, B.E., Sheaff, R.J., Thress, K., Groudine, M., and Roberts, J.M. (1996). Turnover of cyclin E by the ubiquitin-proteasome pathway is regulated by cdk2 binding and cyclin phosphorylation. Genes Dev. *10*, 1979–1990.

Connor, M.K., Kotchetkov, R., Cariou, S., Resch, A., Lupetti, R., Beniston, R.G., Melchior, F., Hengst, L., and Slingerland, J.M. (2003). CRM1/Ran-mediated nuclear export of p27(Kip1) involves a nuclear export signal and links p27 export and proteolysis. Mol. Biol. Cell *14*, 201–213.

Correa-Bordes, J., and Nurse, P. (1995). p25rum1 orders S phase

and mitosis by acting as an inhibitor of the p34Cdc2 mitotic kinase. Cell *83*, 1001–1009.

Dealy, M., Nguyen, K.V.T., Lo, J., Gstaiger, M., Krek, W., Elson, D., Arbeit, J., Kipreos, E.T., and Johnson, R.S. (1999). Loss of Cul1 results in early embryonic lethality and dysregulation of cyclin E. Nat. Genet. *23*, 245–248.

Edgar, B.A., and Orr-Weaver, T.L. (2001). Endoreplication cell cycles: more for less. Cell *105*, 297–306.

Fero, M.L., Rivkin, M., Tasch, M., Porter, P., Carow, C.E., Firpo, E., Polyak, K., Tsai, L.H., Broudy, V., Perlmutter, R.M., et al. (1996). A syndrome of multiorgan hyperplasia with features of gigantism, tumorigenesis, and female sterility in $p27^{Kip1}$-deficient mice. Cell *85*, 733–744.

Fujii, H., Hayama, T., and Kotani, M. (1985). Stimulating effect of natural estrogens on proliferation of hepatocytes in adult mice. Acta Anat. *121*, 174–178.

Hara, T., Kamura, T., Nakayama, K., Oshikawa, K., Hatakeyama, S., and Nakayama, K.I. (2001). Degradation of $p27^{Kip1}$ at the G_0-G_1 transition mediated by a Skp2-independent ubiquitination pathway. J. Biol. Chem. *276*, 48937–48943.

Hatakeyama, S., Kitagawa, M., Nakayama, K., Shirane, M., Matsumoto, M., Hattori, K., Higashi, H., Nakano, H., Okumura, K., Onoe, K., et al. (1999). Ubiquitin-dependent degradation of IκBα is mediated by a ubiquitin ligase Skp1/Cul 1/F-box protein FWD1. Proc. Natl. Acad. Sci. USA *96*, 3859–3863.

Hattori, N., Davies, T.C., Anson-Cartwright, L., and Cross, J.C. (2000). Periodic expression of the cyclin-dependent kinase inhibitor $p57^{Kip2}$ in trophoblast giant cells defines a G2-like gap phase of the endocycle. Mol. Biol. Cell *11*, 1037–1045.

Hengst, L., and Reed, S.I. (1996). Translational control of $p27^{Kip1}$ accumulation during the cell cycle. Science *271*, 1861–1864.

Ishida, N., Hara, T., Kamura, T., Yoshida, M., Nakayama, K., and Nakayama, K.I. (2002). Phosphorylation of $p27^{Kip1}$ on serine 10 is required for its binding to CRM1 and nuclear export. J. Biol. Chem. *277*, 14355–14358.

Kamura, T., Hara, T., Kotoshiba, S., Yada, M., Ishida, N., Imaki, H., Hatakeyama, S., Nakayama, K., and Nakayama, K.I. (2003). Degradation of $p57^{Kip2}$ mediated by SCF^{Skp2}-dependent ubiquitylation. Proc. Natl. Acad. Sci. USA *100*, 10231–10236.

Kiernan, R.E., Emiliani, S., Nakayama, K., Castro, A., Labbe, J.C., Lorca, T., Nakayama, K.I., and Benkirane, M. (2001). Interaction between cyclin T1 and SCF^{SKP2} targets CDK9 for ubiquitination and degradation by the proteasome. Mol. Cell. Biol. *21*, 7956–7970.

Kim, S.Y., Herbst, A., Tworkowski, K.A., Salghetti, S.E., and Tansey, W.P. (2003). Skp2 regulates myc protein stability and activity. Mol. Cell *11*, 1177–1188.

Kitagawa, M., Okabe, T., Ogino, H., Matsumoto, H., Suzuki-Takahashi, I., Kokubo, T., Higashi, H., Saitoh, S., Taya, Y., Yasuda, H., et al. (1993). Butyrolactone I, a selective inhibitor of cdk2 and Cdc2 kinase. Oncogene *8*, 2425–2432.

Kitagawa, M., Hatakeyama, S., Shirane, M., Matsumoto, M., Ishida, N., Hattori, K., Nakamichi, I., Kikuchi, A., Nakayama, K.I., and Nakayama, K. (1999). An F-box protein, FWD1, mediates ubiquitin-dependent proteolysis of β-catenin. EMBO J. *18*, 2401–2410.

Kiyokawa, H., Kineman, R.D., Manova-Todorova, K.O., Soares, V.C., Hoffman, E.S., Ono, M., Khanam, D., Hayday, A.C., Frohman, L.A., and Koff, A. (1996). Enhanced growth of mice lacking the cyclin-dependent kinase inhibitor function of $p27^{Kip1}$. Cell *85*, 721–732.

Koepp, D.M., Schaefer, L.K., Ye, X., Keyomarsi, K., Chu, C., Harper, J.W., and Elledge, S.J. (2001). Phosphorylation-dependent ubiquitination of cyclin E by the SCF^{Fbw7} ubiquitin ligase. Science *294*, 173–177.

Kominami, K., and Toda, T. (1997). Fission yeast WD-repeat protein pop1 regulates genome ploidy through ubiquitin-proteasome-mediated degradation of the CDK inhibitor Rum1 and the S-phase initiator Cdc18. Genes Dev. *11*, 1548–1560.

Li, X., Zhao, Q., Liao, R., Sun, P., and Wu, X. (2003). The SCF^{Skp2} ubiquitin ligase complex interacts with the human replication licensing factor Cdt1 and regulates Cdt1 degradation. J. Biol. Chem. *278*, 30854–30858.

Marti, A., Wirbelauer, C., Scheffner, M., and Krek, W. (1999). Interaction between ubiquitin-protein ligase SCF^{SKP2} and E2F–1 underlies the regulation of E2F–1 degradation. Nat. Cell Biol. *1*, 14–19.

Mendez, J., Zou-Yang, X.H., Kim, S.Y., Hidaka, M., Tansey, W.P., and Stillman, B. (2002). Human origin recognition complex large subunit is degraded by ubiquitin-mediated proteolysis after initiation of DNA replication. Mol. Cell *9*, 481–491.

Minamishima, Y.A., Nakayama, K., and Nakayama, K.I. (2002). Recovery of liver mass without proliferation of hepatocytes after partial hepatectomy in Skp2-deficient mice. Cancer Res. *62*, 995–999.

Miura, M., Hatakeyama, S., Hattori, K., and Nakayama, K.I. (1999). Structure and expression of the gene encoding mouse F-Box protein, Fwd2. Genomics *62*, 50–58.

Moberg, K.H., Bell, D.W., Wahrer, D.C., Haber, D.A., and Hariharan, I.K. (2001). Archipelago regulates Cyclin E levels in Drosophila and is mutated in human cancer cell lines. Nature *413*, 311–316.

Montagnoli, A., Fiore, F., Eytan, E., Carrano, A.C., Draetta, G.F., Hershko, A., and Pagano, M. (1999). Ubiquitination of p27 is regulated by Cdk-dependent phosphorylation and trimeric complex formation. Genes Dev. *13*, 1181–1189.

Nagahama, H., Hatakeyama, S., Nakayama, K., Nagata, M., Tomita, K., and Nakayama, K.I. (2001). Spatial and temporal expression patterns of the cyclin-dependent kinase (CDK) inhibitors $p27^{Kip1}$ and $p57^{Kip2}$ during mouse development. Anat. Embryol. *203*, 77–87.

Nakayama, K., Ishida, N., Shirane, M., Inomata, A., Inoue, T., Shishido, N., Horii, I., Loh, D.Y., and Nakayama, K.I. (1996). Mice lacking $p27^{Kip1}$ display increased body size, multiple organ hyperplasia, retinal dysplasia, and pituitary tumors. Cell *85*, 707–720.

Nakayama, K., Nagahama, H., Minamishima, Y.A., Matsumoto, M., Nakamichi, I., Kitagawa, K., Shirane, M., Tsunematsu, R., Tsukiyama, T., Ishida, N., et al. (2000). Targeted disruption of Skp2 results in accumulation of cyclin E and $p27^{Kip1}$, polyploidy and centrosome overduplication. EMBO J. *19*, 2069–2081.

Nakayama, K.I., Hatakeyama, S., and Nakayama, K. (2001). Regulation of the cell cycle at the G_1-S transition by proteolysis of cyclin E and $p27^{Kip1}$. Biochem. Biophys. Res. Commun. *282*, 853–860.

Nguyen, V.Q., Co, C., and Li, J.J. (2001). Cyclin-dependent kinases prevent DNA re-replication through multiple mechanisms. Nature *411*, 1068–1073.

Pagano, M., Tam, S.W., Theodoras, A.M., Beer-Romero, P., Del Sal, G., Chau, V., Yew, P.R., Draetta, G.F., and Rolfe, M. (1995). Role of the ubiquitin-proteasome pathway in regulating abundance of the cyclin-dependent kinase inhibitor p27. Science *269*, 682–685.

Rodier, G., Montagnoli, A., Marcotullio, D.L., Coulombe, P., Draetta, D.G., Pagano, M., and Meloche, S. (2001). p27 cytoplasmic localization is regulated by phosphorylation on Ser10 and is not a prerequisite for its proteolysis. EMBO J. *20*, 6672–6682.

Sheaff, R.J., Groudine, M., Gordon, M., Roberts, J.M., and Clurman, B.E. (1997). Cyclin E-CDK2 is a regulator of $p27^{Kip1}$. Genes Dev. *11*, 1464–1478.

Shirane, M., Harumiya, Y., Ishida, N., Hirai, A., Miyamoto, C., Hatakeyama, S., Nakayama, K.I., and Kitagawa, M. (1999). Down-regulation of $p27^{Kip1}$ by two mechanisms, ubiquitin-mediated degradation and proteolytic processing. J. Biol. Chem. *274*, 13886–13893.

Singer, J.D., Gurian-West, M., Clurman, B., and Roberts, J.M. (1999). Cullin-3 targets cyclin E for ubiquitination and controls S phase in mammalian cells. Genes Dev. *13*, 2375–2387.

Stern, B., and Nurse, P. (1996). A quantitative model for the Cdc2 control of S phase and mitosis in fission yeast. Trends Genet. *12*, 345–350.

Strohmaier, H., Spruck, C.H., Kaiser, P., Won, K.A., Sangfelt, O., and Reed, S.I. (2001). Human F-box protein hCdc4 targets cyclin E for proteolysis and is mutated in a breast cancer cell line. Nature *413*, 316–322.

Sutterluty, H., Chatelain, E., Marti, A., Wirbelauer, C., Senften, M.,

Muller, U., and Krek, W. (1999). p45^{SKP2} promotes p27^{Kip1} degradation and induces S phase in quiescent cells. Nat. Cell Biol. *1*, 207–214.

Tedder, T.F., and Isaacs, C.M. (1989). Isolation of cDNAs encoding the CD19 antigen of human and mouse B lymphocytes. J. Immunol. *143*, 712–717.

Tedesco, D., Lukas, J., and Reed, S.I. (2002). The pRb-related protein p130 is regulated by phosphorylation-dependent proteolysis via the protein-ubiquitin ligase SCF^{Skp2}. Genes Dev. *16*, 2946–2957.

Th'ng, J.P., Wright, P.S., Hamaguchi, J., Lee, M.G., Norbury, C.J., Nurse, P., and Bradbury, E.M. (1990). The FT210 cell line is a mouse G2 phase mutant with a temperature-sensitive CDC2 gene product. Cell *63*, 313–324.

Tomoda, K., Kubota, Y., and Kato, J. (1999). Degradation of the cyclin-dependent-kinase inhibitor p27^{Kip1} is instigated by Jab1. Nature *398*, 160–165.

Tsunematsu, R., Nakayama, K., Oike, Y., Nishiyama, M., Ishida, N., Hatakeyama, S., Bessho, Y., Kageyama, R., Suda, T., and Nakayama, K.I. (2004). Mouse Fbw7/Sel-10/Cdc4 is required for notch degradation during vascular development. J. Biol. Chem. *279*, 9417–9423.

Tsvetkov, L.M., Yeh, K.H., Lee, S.J., Sun, H., and Zhang, H. (1999). p27^{Kip1} ubiquitination and degradation is regulated by the SCF^{Skp2} complex through phosphorylated Thr187 in p27. Curr. Biol. *9*, 661–664.

Vlach, J., Hennecke, S., and Amati, B. (1997). Phosphorylation-dependent degradation of the cyclin-dependent kinase inhibitor p27. EMBO J. *16*, 5334–5344.

von der Lehr, N., Johansson, S., Wu, S., Bahram, F., Castell, A., Cetinkaya, C., Hydbring, P., Weidung, I., Nakayama, K., Nakayama, K.I., et al. (2003). The F-box protein Skp2 participates in c-Myc proteasomal degradation and acts as a cofactor for c-Myc-regulated transcription. Mol. Cell *11*, 1189–1200.

Wang, Y., Penfold, S., Tang, X., Hattori, N., Riley, P., Harper, J.W., Cross, J.C., and Tyers, M. (1999). Deletion of the Cul1 gene in mice causes arrest in early embryogenesis and accumulation of cyclin E. Curr. Biol. *9*, 1191–1194.

Won, K.A., and Reed, S.I. (1996). Activation of cyclin E/CDK2 is coupled to site-specific autophosphorylation and ubiquitin-dependent degradation of cyclin E. EMBO J. *15*, 4182–4193.

Yu, Z.K., Gervais, J.L., and Zhang, H. (1998). Human CUL-1 associates with the SKP1/SKP2 complex and regulates p21(CIP1/WAF1) and cyclin D proteins. Proc. Natl. Acad. Sci. USA *95*, 11324–11329.

Zybina, E.V., and Zybina, T.G. (1996). Polytene chromosomes in mammalian cells. Int. Rev. Cytol. *165*, 53–119.

Analysis of Small Human Proteins Reveals the Translation of Upstream Open Reading Frames of mRNAs

Masaaki Oyama,[1] Chiharu Itagaki,[2] Hiroko Hata,[3] Yutaka Suzuki,[1] Tomonori Izumi,[2] Tohru Natsume,[4] Toshiaki Isobe,[2] and Sumio Sugano[1,5]

[1]*Human Genome Center, Division of* [2]*Proteomics Research and* [3]*Cancer Genomics, Institute of Medical Science, University of Tokyo, Minato-ku, Tokyo 108-8639, Japan;* [4]*National Institute of Advanced Industrial Science and Technology, Biological Information Research Center (JBIRC), Koutoh-ku, Tokyo 135-0064, Japan*

To find novel short coding sequences from accumulated full-length cDNA sequences, proteomic analysis of small proteins expressed in human leukemia K562 cells was performed using high-resolution nanoflow liquid chromatography coupled with electrospray ionization tandem mass spectrometry. Our analysis led to the identification of 54 proteins not more than 100 amino acids in length, including four novel ones. These novel short coding sequences were all located upstream of the longest open reading frame (ORF) of the corresponding cDNA. Our findings indicate that the translation of short ORFs occurs in vivo whether or not there exists a longer coding region in the downstream of the mRNA. This investigation provides the first direct evidence of translation of upstream ORFs in human cells, which could greatly change the current outline of the human proteome.

[Supplemental material is available online at www.genome.org.]

In parallel with human genome sequencing projects (Lander et al. 2001; Venter et al. 2001), the accumulation of sequence data of human full-length cDNAs has also been proceeding. The "RefSeq collection" (NCBI) provides us with representative resources of curated human full-length cDNAs, and the protein-coding sequence (CDS) of each cDNA is defined in the RefSeq database (Pruitt and Maglott 2001). Now a total of 19,995 proteins are stored in the RefSeq curated human protein database (as of January 27, 2004), and 19,271 (96.4%) of them are longer than 100 amino acids. This indicates that small proteins with ≦100 amino acids are only a limited fraction of all the proteins annotated in the RefSeq database.

According to the typical translation model, a 40S ribosomal subunit is first recruited to the cap structure of mRNA and linearly scans the 5′-UTR for the initiator ATG. When it recognizes the initiator ATG, it pauses until a large 60S subunit joins, and the complete ribosomal complex starts translation (Kozak 1989). Therefore, the most upstream ORF should be translated according to this model, much more with a good context around its ATG codon as previously analyzed (Kozak 1999). Some previous studies have reported that the short ORF in the 5′-untranslated region (UTR) functions as a regulator of the translation of its downstream CDS (Morris and Geballe 2000; Meijer and Thomas 2002). It has been considered that such translational control would be limited to some genes or conditions. However, the previous large-scale analyses focusing on the 5′-UTRs of human full-length cDNA sequences showed that 41%–49% of them had at least one ATG codon upstream of the CDS (Peri and Pandey 2001; Yamashita et al. 2003). This means that there are potential short coding regions in the 5′-UTRs of many genes if this classical model, indeed, represents a general mechanism of translation initiation. To our knowledge, few reports have presented evidence of the translation of upstream ORFs in vivo (Diba et al. 2001). Although there are also some mechanisms by which the ribosomal complex may evade the translation from the first ATG codon, such as leaky scanning (Kozak 1999) and IRES (internal ribosome entry site)-dependent translation (Meijer and Thomas 2002), we expect that the small proteins encoded by upstream ORFs in 5′-UTRs exist in vivo.

With a view to finding novel short upstream CDSs in accumulated cDNA sequences, we performed a proteomic analysis of small proteins expressed in vivo using direct nanoflow liquid chromatography (LC) coupled with the electrospray ionization (ESI)–tandem mass spectrometry (MS/MS) system (Natsume et al. 2002). This LC instrument can separate peptides and introduce them into a mass spectrometer with limited diffusion, leading to more sensitive detection than can be achieved with conventional LC systems. We aimed to identify novel short CDSs by searching not only against the RefSeq curated cDNA database but also against our in-house FLJ-unique cDNA data set, which contained as many as >10,000 full-length cDNA sequences that had no hit against the RefSeq cDNAs (Ota et al. 2004).

Here we report the proteomic analysis of small proteins (≦100 amino acids in length) expressed in human chronic myelogenous leukemia K562 cells. Our analysis led to the identification of 54 proteins in total, including four novel ones. Very intriguingly, these novel small proteins were all derived from the short ORFs in the presumed 5′-UTRs.

RESULTS

To carry out a proteomic analysis of small proteins expressed in K562 cells, we prepared the samples for mass spectrometric analysis by two different methods. Small proteins were isolated by either fractionation through SDS-PAGE or acid extraction. For the proteins resolved by SDS-PAGE, the part of the gel corresponding to the low molecular weight (<~17 kDa) was excised, and the proteins trapped in the gel were digested with proteolytic enzymes (see "MS Sample Preparation 1" in Methods). On the

[5]**Corresponding author.**
E-MAIL ssugano@ims.u-tokyo.ac.jp; FAX 81-3-5449-5416.
Article and publication are at http://www.genome.org/cgi/doi/10.1101/gr.2384604.

14:2048–2052 ©2004 by Cold Spring Harbor Laboratory Press ISSN 1088-9051/04; www.genome.org

Table 1. Novel Short CDSs Identified by Searching Against Human cDNAs

GenBank Accession	Length (bp)	Novel CDS position[a]	Novel CDS length[a] (amino acids)	Novel CDS initiator ATG[a]	Identified peptide[b]	Longest ORF position[a]	Longest ORF length[a] (amino acids)
RefSeq cDNAs							
NM_005770	1408	941...1120	59	6th	QRDSEIMQQK RDDGLSAAAR	1023...1319	98
NM_015532	4107	12...272	86	1st	QPQPAQNVLAAPR GLGAAEFGGAAGNVEAPGETFAQR	127...1233	368
NM_016215	1545	150...401	83	1st	ATPGLQQHQQPPGPGR (N-terminus acetylated)	316...1137	273
FLJ cDNAs							
AK057257	1904	23...280	85	1st	LLPLGASPAGVVGGGLAPPR	654...1013	119

[a]Each data is based on the sequence information of the corresponding cDNA.
[b]Peptides identified from MS samples (see Methods).

other hand, the small proteins enriched by extraction in acid solution were digested directly without PAGE separation (see "MS Sample Preparation 2" in Methods). After concentrating the peptide mixtures prepared by each of the two methods, we applied them to the nanoflow LC-MS/MS system.

We first tried identifying small proteins (≦100 amino acids in length) by searching against the RefSeq curated human "protein" database (NCBI). Accordingly, 36 proteins were identified from the gel-separated samples, and 23 proteins were identified from the acid-extracted samples. In total, 50 proteins (with nine overlaps) were identified out of 724 proteins (≦100 amino acids in length) stored in the RefSeq protein database (as of January 27, 2004; see Supplemental table). The range of amino acid length of the identified proteins was from 44 to 100. The list included various kinds of small proteins, such as ribosomal proteins, transporters, transcriptional regulators, cell cycle regulators, spliceosome components, and proteins involved in energy metabolism. We also found several function-unknown proteins expressed in K562 cells.

Next, to search for novel short CDSs that were not annotated in the RefSeq curated human protein database, all the MS/MS data that had no hit against RefSeq proteins were then searched against all the ORFs (in all three reading frames) of the RefSeq curated cDNA database and of our in-house "FLJ-unique" cDNA data set. As a result, four novel translated ORFs were identified (Table 1). Three of them were derived from RefSeq cDNAs, whereas the other was from an FLJ cDNA. As an example, the MS/MS spectrum matching the NM_015532 novel short CDS is shown in Figure 1A. An intense string of as many as 10 ions from the *y* ion series resulted in an excellent match for the corresponding peptide. The other peptides listed in Table 1 also yielded comparable search results, indicating the translation of these short ORFs. Moreover, the identification of the NM_015532 novel short CDS was also shown by matching of another peptide (Fig. 1B). This evidence gives us additional support for the presence of this novel CDS, which is also the case with the NM_005770 novel CDS (Table 1).

In Figure 2, we show the location of these novel CDSs within each corresponding cDNA. Interestingly, all the novel CDSs are located upstream of the longest ORF. Three of them overlap with each longest ORF, whereas the other is distant. A nucleotide deletion or insertion arising from a sequencing error can cause an erroneous short ORF to be produced from the longest ORF by a frameshift in the reading frame. Also, there might be splicing variants that can result in the fusion of the short ORF to the longest ORF. Therefore, careful confirmation of the corresponding nucleotide sequences was needed.

Here we tried aligning the EST data corresponding to the NM_015532 novel short CDS. As this novel short CDS is located near the 5′-end of the mRNA as shown in Figure 2, we aligned the 5′-end cDNA sequence data provided by the "oligo-capping" method, which was previously established by us for collecting accurate 5′-end nucleotide sequences from the mRNA start site (Suzuki et al. 1997, 2001). The multiple alignment of the sequence data of 11 corresponding cDNAs from 10 different resources showed no alternative splicing pattern over the entire region of this short CDS and a complete match for NM_015532

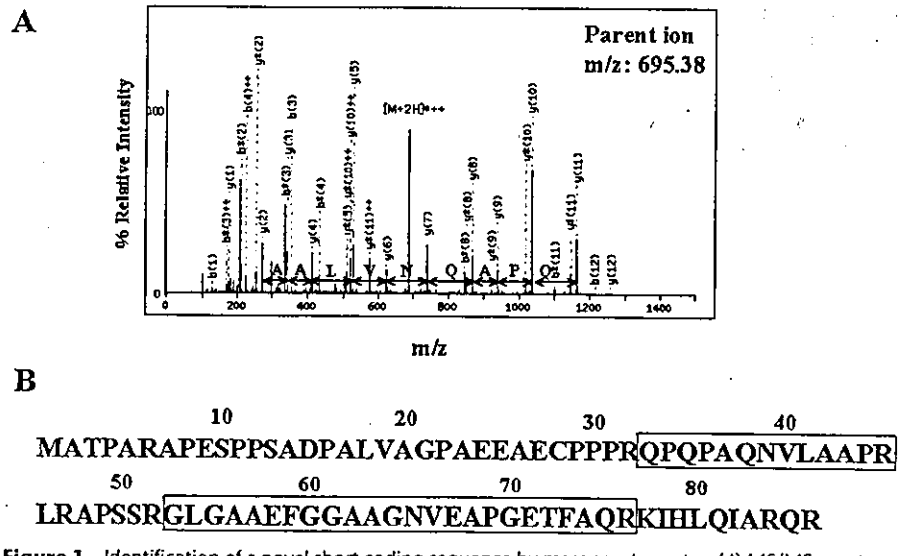

Figure 1 Identification of a novel short coding sequence by mass spectrometry. (*A*) MS/MS spectrum corresponding to the peptide QPQPAQNVLAAPR at *m/z* 695.38 derived from the NM_015532 ORF. The corresponding amino acid differences based on a series of as many as 10 continuous *y* ions are represented. An asterisk (*) indicates an ion that has lost ammonia from its side chain. (*B*) Amino acid sequence of the NM_015532 upstream short ORF. The identified peptides are surrounded by rectangles.

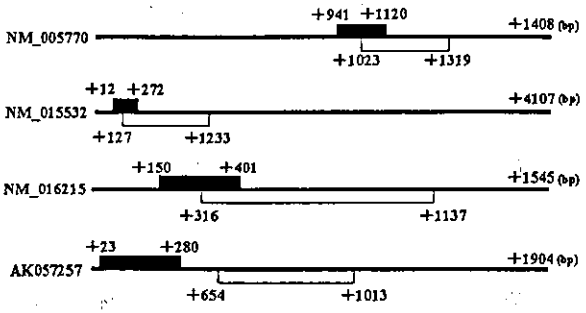

Figure 2 Location of the identified novel CDS (black box) and the longest ORF (white box) of each full-length cDNA. The numbers indicate the positions from each full-length cDNA start site.

around the termination codon as shown in Figure 3A (the detailed sequence data can be seen at DataBase of Transcriptional Start Sites; DBTSS; Release 3.0; http://dbtss.hgc.jp/; Suzuki et al. 2002). As for the other three novel short CDSs, accumulated EST evidence showed that there were also no frameshift or alternative splicing variants that indicated the existence of a fused and longer ORF.

Furthermore, comparative sequence analysis of the NM_015532 novel CDS and its mouse ortholog counterpart showed 86% DNA identity with 16 conservative changes and 15 nonconservative ones over the aligned ORFs (261 nt in length), resulting in 85% identity and 95% similarity across the entire length of their deduced amino acid sequences (86 amino acids in length; Fig. 3B). Evidence of such a high degree of evolutionary sequence conservation indicates functional constraint on this novel short CDS. Table 2 shows that the NM_005770 upstream CDS is also functionally constrained, whereas that of NM_016215 is relatively loosened. As for that of NM_005770, the previous study has indicated that it shares homology with the protein encoded by a candidate modifying gene for spinal muscular atrophy (Scharf et al. 1998).

DISCUSSION

Our proteomic analysis of small proteins expressed in K562 cells has enabled us to reveal the existence of the proteins encoded by upstream ORFs in 5′-UTRs. To our knowledge, this is the first direct evidence of translation of upstream ORFs in human cells. There were only four upstream short CDSs identified in our analysis, while leading to the identification of 50 RefSeq-annotated proteins. One of the reasons might be that some parts of upstream ORFs would not be efficiently translated in K562 cells because of the poor Kozak's context around their ATG codons. The previous studies indicated that 37%–57 % of the upstream ATGs in the 5′-UTRs had an unfavorable Kozak's context around the ATG codon (Kozak 1987; Suzuki et al. 2000). Secondly, our recent analysis also indicated that approximately three-fourths of the upstream ORFs analyzed were shorter than 40 amino acids (Yamashita et al. 2003). Considering that the smallest protein identified from the RefSeq curated database is 44 amino acids in length, it is very possible that such very small proteins were out of the detectable range in our analysis. They would be lost while preparing the samples for MS analysis.

However, these reasons from the statistical point of view cannot by themselves fully explain why there were no more than four proteins identified among thousands of upstream ORFs. One of the other possibilities is that many of the proteins derived from upstream ORFs might be selectively proteolyzed in the cells. Secondly, there might be some mechanisms that allow ribosomes to avoid the translation of upstream ORFs. Although IRES-dependent translation can permit ribosomes to directly enter a downstream site without encountering an upstream ATG, the previous studies have estimated that this mechanism would be applied to a limited fraction of genes (Meijer and Thomas 2002). There might exist another mechanism that enables ribosomes to escape the translation of an upstream ORF. Thirdly, the transcripts expressed in K562 cells might not reflect the corresponding cDNA sequences stored in the database. Our previous large-scale analysis on the 5′-UTRs has shown that the transcription start sites of many genes are more dispersed than was previously believed (Suzuki et al. 2001). Thus, it is likely that there are many genes whose transcripts in K562 cells have a shorter 5′-UTR that lacks an upstream ATG. Further analysis will be required to clarify this point.

Mapping of the novel short CDSs onto the corresponding full-length cDNAs indicates that three of these CDSs (but not the NM_005770 short CDS) use the most upstream ATG as an initiation codon (Table 1). As to the NM_005770 short CDS, the sixth ATG corresponds to its translation start site on the cDNA sequence of NM_005770. However, the accumulated oligo-capped 5′-end cDNA data of this gene obtained from various types of human tissues and cell lines uniformly showed the existence of the short transcript form whose first ATG corresponded to the initiation codon of this novel CDS (see the sequence data at DBTSS [Release 3.0]; http://dbtss.hgc.jp/). This indicates that this

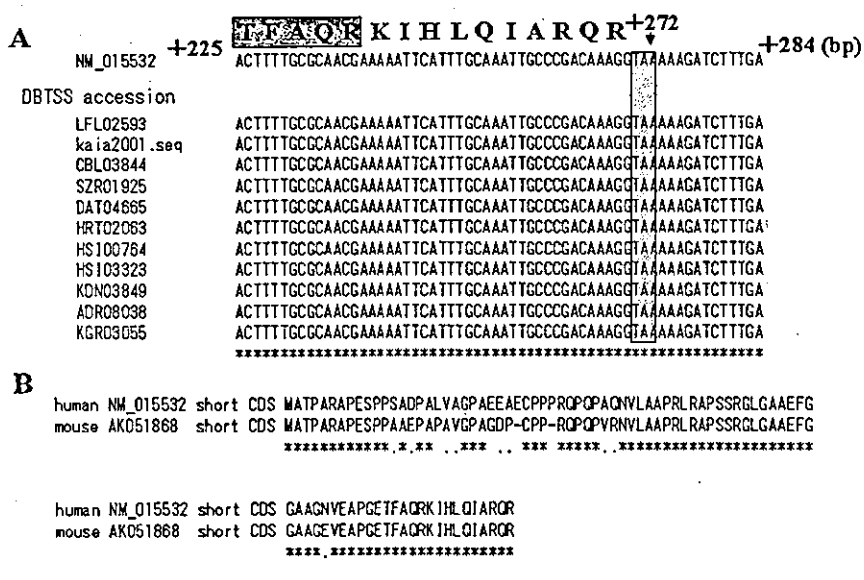

Figure 3 Sequence analysis of the NM_015532 novel short CDS. (*A*) Multiple alignment of the 5′-end EST data around the termination codon. The dark box shows the C terminus of the secondarily identified peptide. An asterisk (*) indicates a complete sequence match between the RefSeq cDNA (NM_015532) and all the EST data. The shaded box indicates the termination codon of this short CDS. (*B*) Alignment of the NM_015532 short CDS with its mouse ortholog at the amino acid level. The amino acid sequence of the mouse ortholog was deduced from the sequence (from +13 to +267) of AK051868. An asterisk (*) and a dot (.) indicate identity and similarity in amino acid sequence, respectively. (DBTSS) DataBase of Transcriptional Start Sites (http://dbtss.hgc.jp/; Suzuki et al. 2002).

Table 2. Sequence Conservation of the Upstream CDS and the Longest ORF of Each RefSeq cDNA

RefSeq ID	Upstream CDS[a] (%)	Longest ORF[a] (%)	Longest ORF RefSeq definition
NM_005770	100	94	Small EDRK-rich factor 2 (SERF2)
NM_015532	95	89	Glutamate receptor, ionotropic, *N*-methyl D-aspartate-like 1A (GRINL1A)
NM_016215	71	92	EGF-like domain, multiple 7 (EGFL7)

[a]Each value represents the rate of similar amino acid residues over the entire region in the alignment of the human protein sequence with that of its mouse ortholog using CLUSTAL W (http://www.ddbj.nig.ac.jp/E-mail/clustalw-j.html).
Each amino acid sequence was deduced from the corresponding nucleotide sequence region of each cDNA. The mouse orthologous regions were extracted from the cDNA data below.
NM_005770 [upstream CDS: NM_011354 (+19–+198); longest ORF: NM_011354 (+101–+397)].
NM_015532 [upstream CDS: AK051868 (+13–+267); longest ORF: AK051868 (+122–+1222)].
NM_016215 [upstream CDS: NM_198724 (+125–+367); longest ORF: NM_198724 (+294–+1130)].

gene has two alternative transcript forms and the majority is the shorter one. Thus, it is very possible that translation of this short CDS initiates from the first ATG of the corresponding short transcript in K562 cells. In the conventional mechanism of translation initiation, the first ATG should be recognized as an initiation codon (the first ATG rule; Kozak 1989). Our finding of these four upstream CDSs is supportive evidence for this rule. In addition, the classification on the probable translation initiation sites of the small RefSeq proteins identified in our analysis shows that 42 (84%) out of the 50 listed proteins use the first ATG as an initiation codon (see Supplemental table). These results indicate that the small proteins relatively abundant in K562 cells were mainly produced according to the first ATG rule. Much more evidence of the translation of upstream ORFs could demonstrate that the translation from the first ATG generally occurs, indeed.

As for NM_015532, NM_016215, and AK057257, the splicing junctions are left downstream of the translation termination site of each upstream CDS. The nonsense-mediated decay (NMD) pathway triggers the degradation of the transcripts holding exon junction complexes (EJCs), which should be removed by a migrating ribosome during the process of translation (Maquat 2004). Therefore, these transcripts are considered to be susceptible to degradation by this pathway. Translation of the downstream longest ORF can protect the transcripts from degradation through removal of the remaining EJCs. As described in Table 2, the longest ORFs of the three RefSeq genes are highly conserved between human and mouse and the mouse ortholog corresponding to that of NM_016215 has been characterized as an endothelial repressor of smooth muscle cell migration (Soncin et al. 2003). As for the longest ORF of AK057257, it shares strong homology with α-tubulin, which also indicates its functionality (data not shown). The investigation on whether the translation of these downstream longest ORFs occurs in K562 cells will be needed to consider this point.

Further explorations based on mass spectrometric analysis will lead to the identification of more short CDSs through improvement of the method for the fractionation of small proteins or through sophistication of the LC system to acquire more MS/MS spectra. The analysis of small proteins expressed in other cultured cells or tissues will also reveal the existence of those expressed in a tissue-specific manner. Accumulating evidence of the translation of upstream short ORFs will make it possible for us to obtain a clearer outline of translatable regions of numerous mRNA species and help us to determine the real size and contents of the human proteome.

METHODS

Cell Culture

Human chronic myelogenous leukemia K562 cells were grown in RPMI/10% dialyzed FCS to a density of 1×10^6 cells/mL, harvested, and washed three times with PBS.

MS Sample Preparation 1

Harvested K562 cells (5×10^6) were lysed in lysis buffer (50 mM Tris-HCl at pH 7.6, 0.5 % [w/v] Triton X-100, 150 mM NaCl) supplemented with protease inhibitor cocktail Complete mini (Boerhinger Mannheim) and centrifuged for 10 min at 12,000 rpm at 4°C. The obtained supernatant was separated by SDS-PAGE with a 14% lower gel. The part of the lane corresponding to <~17 kDa was cut into small pieces, and the proteins in the gel pieces were digested overnight at 37°C with 25 pmoles of trypsin, sequencing-grade (Roche Diagnostics) in 20 mM Tris-HCl (pH 8.8). These procedures were performed according to the previously described method (Shevchenko et al. 1996). The peptides were extracted from the gel pieces with a total of 300 µL of 50% (v/v) acetonitrile/5% formic acid by sonication and concentrated to ~50 µL using a centrifugal vacuum concentrator. After the sample was desalted using a ZipTip (C_{18}; Millipore), the peptides were eluted with 50 µL of 70% (v/v) acetonitrile/0.1% (v/v) formic acid and again concentrated to a final volume of 5 µL.

MS Sample Preparation 2

Harvested K562 cells (5×10^8) were boiled for 10 min at 95°C to inactivate proteases. The cells were then lysed in 1 M acetic acid using a Dounce homogenizer on ice and centrifuged for 10 min at 12,000 rpm at 4°C. After eliminating salts and other low-molecular-weight contaminants from the supernatant using a PD-10 Column (Amersham Biosciences) filled with Sephadex G-25, one-hundredth of the protein-enriched fraction was digested overnight at 37°C with 25 pmoles of trypsin in 20 mM Tris-HCl (pH 8.8). After the sample was desalted using a ZipTip (C_{18}), it was processed in the same way as described above for MS Sample Preparation 1.

Automated Nanoflow LC-MS/MS Analysis and Protein Identification by Database Search

The peptide mixtures were analyzed using a high-resolution nanoflow reversed-phase capillary LC coupled with an electrospray quadrupole time-of-flight (Q-TOF) tandem mass spectrometer (Q-Tof-2; Micromass Ltd.). The acquired MS/MS spectra were converted to text files of peak lists and processed using the Mascot algorithm (Matrix Science Ltd.) with a maximum tolerance of 500 ppm in MS data and 0.5 Da in MS/MS data against each database. The RefSeq databases were downloaded periodically from the NCBI ftp site (ftp://ftp.ncbi.nih.gov/refseq/). The FLJ-unique cDNA data set was prepared and characterized as previously described (Ota et al. 2004). The results based on the RefSeq data were finally reviewed according to the RefSeq information as of March 5, 2004.

ACKNOWLEDGMENTS

We thank T. Hasui for his technical support in the database construction. We are grateful to E. Nakajima for her critical reading of the manuscript. This work was supported by a Grant-in-Aid for Scientific Research on Priority Areas from the Ministry of Education, Science, Sports and Culture of Japan.

REFERENCES

Diba, F., Watson, C.S., and Gametchu, B. 2001. 5'UTR sequences of the glucocorticoid receptor 1A transcript encode a peptide associated with translational regulation of the glucocorticoid receptor. *J. Cell Biochem.* **81:** 149–161.

Kozak, M. 1987. An analysis of 5'-noncoding sequences from 699 vertebrate messenger RNAs. *Nucleic Acids Res.* **15:** 8125–8148.

———. 1989. The scanning model for translation: An update. *J. Cell Biol.* **108:** 229–241.

———. 1999. Initiation of translation in prokaryotes and eukaryotes. *Gene* **234:** 187–208.

Lander, E.S., Linton, L.M., Birren, B., Nusbaum, C., Zody, M.C., Baldwin, J., Devon, K., Dewar, K., Doyle, M., FitzHugh, W., et al. 2001. Initial sequencing and analysis of the human genome. *Nature* **409:** 860–921.

Maquat, L.E. 2004. Nonsense-mediated mRNA decay: Splicing, translation and mRNP dynamics. *Nat. Rev. Mol. Cell Biol.* **5:** 89–99.

Meijer, H.A. and Thomas, A.A. 2002. Control of eukaryotic protein synthesis by upstream open reading frames in the 5'-untranslated region of an mRNA. *Biochem. J.* **367:** 1–11.

Morris, D.R. and Geballe, A.P. 2000. Upstream open reading frames as regulators of mRNA translation. *Mol. Cell. Biol.* **20:** 8635–8642.

Natsume, T., Yamauchi, Y., Nakayama, H., Shinkawa, T., Yanagida, M., Takahashi, N., and Isobe, T. 2002. A direct nanoflow liquid chromatography–tandem mass spectrometry system for interaction proteomics. *Anal. Chem.* **74:** 4725–4733.

Ota, T., Suzuki, Y., Nishikawa, T., Otsuki, T., Sugiyama, T., Irie, R., Wakamatsu, A., Hayashi, K., Sato, H., Nagai, K., et al. 2004. Complete sequencing and characterization of 21,243 full-length human cDNAs. *Nat. Genet.* **36:** 40–45.

Peri, S. and Pandey, A. 2001. A reassessment of the translation initiation codon in vertebrates. *Trends Genet.* **17:** 685–687.

Pruitt, K.D. and Maglott, D.R. 2001. RefSeq and LocusLink: NCBI gene-centered resources. *Nucleic Acids Res.* **29:** 137–140.

Scharf, J.M., Endrizzi, M.G., Wetter, A., Huang, S., Thompson, T.G., Zerres, K., Dietrich, W.F., Wirth, B., and Kunkel, L.M. 1998. Identification of a candidate modifying gene for spinal muscular atrophy by comparative genomics. *Nat. Genet.* **20:** 83–86.

Shevchenko, A., Wilm, M., Vorm, O., and Mann, M. 1996. Mass spectrometric sequencing of proteins silver-stained polyacrylamide gels. *Anal. Chem.* **68:** 850–858.

Soncin, F., Mattot, V., Lionneton, F., Spruyt, N., Lepretre, F., Begue, A., and Stehelin, D. 2003. VE-statin, an endothelial repressor of smooth muscle cell migration. *EMBO J.* **22:** 5700–5711.

Suzuki, Y., Yoshitomo-Nakagawa, K., Maruyama, K., Suyama, A., and Sugano, S. 1997. Construction and characterization of a full length-enriched and a 5'-end-enriched cDNA library. *Gene* **200:** 149–156.

Suzuki, Y., Ishihara, D., Sasaki, M., Nakagawa, H., Hata, H., Tsunoda, T., Watanabe, M., Komatsu, T., Ota, T., Isogai, T., et al. 2000. Statistical analysis of the 5' untranslated region of human mRNA using "Oligo-Capped" cDNA libraries. *Genomics* **64:** 286–297.

Suzuki, Y., Taira, H., Tsunoda, T., Mizushima-Sugano, J., Sese, J., Hata, H., Ota, T., Isogai, T., Tanaka, T., Morishita, S., et al. 2001. Diverse transcriptional initiation revealed by fine, large-scale mapping of mRNA start sites. *EMBO Rep.* **2:** 388–393.

Suzuki, Y., Yamashita, R., Nakai, K., and Sugano, S. 2002. DBTSS: DataBase of human transcriptional start sites and full-length cDNAs. *Nucleic Acids Res.* **30:** 328–331.

Venter, J.C., Adams, M.D., Myers, E.W., Li, P.W., Mural, R.J., Sutton, G.G., Smith, H.O., Yandell, M., Evans, C.A., Holt, R.A., et al. 2001. The sequence of the human genome. *Science* **291:** 1304–1351.

Yamashita, R., Suzuki, Y., Nakai, K., and Sugano, S. 2003. Small open reading frames in 5' untranslated regions of mRNAs. *C.R. Biol.* **326:** 987–991.

WEB SITE REFERENCES

ftp://ftp.ncbi.nih.gov/refseq/; NCBI RefSeq ftp site.

http://dbtss.hgc.jp/; DBTSS: DataBase of human Transcriptional Start Sites.

http://www.ddbj.nig.ac.jp/E-mail/clustalw-j.html; CLUSTAL W.

Received January 23, 2004; accepted in revised form April 9, 2004.

THE JOURNAL OF BIOLOGICAL CHEMISTRY
Vol. 279, No. 3, Issue of January 16, pp. 1607–1614, 2004
Printed in U.S.A.

Human Fibrillarin Forms a Sub-complex with Splicing Factor 2-associated p32, Protein Arginine Methyltransferases, and Tubulins α3 and β1 That Is Independent of Its Association with Preribosomal Ribonucleoprotein Complexes*[S]

Received for publication, May 28, 2003, and in revised form, October 16, 2003
Published, JBC Papers in Press, October 28, 2003, DOI 10.1074/jbc.M305604200

Mitsuaki Yanagida‡§¶, Toshiya Hayano‡§, Yoshio Yamauchi§‖, Takashi Shinkawa‖, Tohru Natsume, Toshiaki Isobe§‖, and Nobuhiro Takahashi‡§‡‡**

*From the ‡Department of Applied Biological Science, and Department of Biotechnology, United Graduate School of Agriculture, Tokyo University of Agriculture and Technology, 3-5-8 Saiwai-cho, Fuchu-shi, Tokyo 183-8509, the §Integrated Proteomics System Project, Pioneer Research on Genome the Frontier, Ministry of Education, Culture, Sports, Science & Technology of Japan, the ‖Laboratory of Biochemistry, Graduate School of Science, Tokyo Metropolitan University, 1-1 Minami-ohsawa, Hachiouji, Tokyo 192-0397, and the **National Institutes of Advanced Industrial Science and Technology, Biological Information Research Center, 2-41-6 Ohmi, Kohtoh-ku, Tokyo 135-0064, Japan*

Fibrillarin (FIB, Nop1p in yeast) is an RNA methyltransferase found not only in the fibrillar region of the nucleolus but also in Cajal bodies. FIB is essential for efficient processing of preribosomal RNA during ribosome biogenesis, although its precise function in this process and its role in Cajal bodies remain uncertain. Here, we demonstrate that the human FIB N-terminal glycine- and arginine-rich domain (residues 1–77) and its spacer region 1 (78–132) interact with splicing factor 2-associated p32 (SF2A-p32) and that the FIB methyltransferase-like domain (133–321) interacts with protein-arginine methyltransferase 5 (PRMT5, Janus kinase-binding protein 1). We also show that these proteins associate with several additional proteins, including PRMT1, tubulin α3, and tubulin β1 to form a sub-complex that is principally independent of the association of FIB with preribosomal ribonucleoprotein complexes that co-immunoprecipitate with the sub-complex in human cells expressing FLAG-tagged FIB. Based on the physical association of FIB with SF2A-p32 and PRMTs, as well as the other reported results, we propose that FIB may coordinate both RNA and protein methylation during the processes of ribosome biogenesis in the nucleolus and RNA editing such as small nuclear (nucleolar) ribonucleoprotein biogenesis in Cajal bodies.

Fibrillarin (FIB)[1] is the most abundant protein in the fibrillar regions of the nucleolus where ribosomal RNA transcription and early preribosomal RNA (pre-rRNA) processing take place (1, 2). FIB is also found in Cajal bodies, subnuclear organelles that contain distinct components involved in RNA transcription and editing such as mRNA splicing and small nuclear (nucleolar) ribonucleoprotein (sn(o)RNP) biogenesis (3, 4). FIB is a component of a ribonucleoprotein (RNP) complex that contains U3, U8, and U13 small nucleolar RNAs that exhibit consensus sequence elements denoted box C (5′-UGAUGA-3′) and box D (5′-CUGA-3′) (5). The FIB RNP associates with Nop56p, Nop5p/58p, and a 15.5-kDa protein (a counterpart of yeast Snu13p) to form box C/D snoRNP complexes that function in site-specific 2′-*O*-methylation of pre-rRNA (6–9). FIB is the methyltransferase that catalyzes this 2′-*O*-methylation (10).

FIB, or Nop1p in the yeast *Saccharomyces cerevisiae*, is highly conserved in eukaryotes with respect to sequence, structure, and function (11–17). Deletion of the *Nop1* gene in yeast results in inhibition of 2′-*O*-ribose methylation and pre-rRNA processing at sites A_0 to A_2, indicating that Nop1p is directly involved in both pre-rRNA methylation and processing and ultimately in ribosome assembly (18). Although human FIB is the functional homolog of yeast Nop1p, it only partially complements a yeast nop1-defective mutant (15). Human FIB is a nucleolar autoantigen for the non-hereditary immune disease scleroderma (14). FIB co-localizes with the survival motor neuron (SMN) gene product in both nucleoli and Cajal bodies/gems of primary neurons (19, 20). SMN is linked to one of the most common inheritable causes of childhood mortality, spinal muscular atrophy (19). In fact, a direct interaction between FIB and SMN has been demonstrated, although no functional basis for this interaction has been established, including any involvement of FIB in the pathogenesis of spinal muscular atrophy. Another protein, the nuclear DEAD box protein p68, an RNA-dependent ATPase and RNA helicase, co-localizes with FIB specifically in nascent nucleoli during telophase (21). As with SMN, no physiological role of its interaction with FIB has been established.

Human FIB (~36 kDa) comprises 321 amino acids and three structural domains (14) and is 66% identical to yeast Nop1p. The N-terminal 80 residues comprise a glycine- and arginine-rich (GAR) domain (14) that is also present in Nop1p and *Xenopus* FIB (Fig. 1) but not in *Tetrahymena* FIB (17) or *Methanococcus jannaschii* FIB (22). The GAR domain is methylated at arginine residues, although the arginine methyltransferase responsible for *in vivo* methylation has not been identified (23, 24). The GAR domain is responsible for the interaction

* This work was supported by a Pioneer Research grant on Genome the Frontier from the Ministry of Education, Culture, Sports, Science, & Technology of Japan. The costs of publication of this article were defrayed in part by the payment of page charges. This article must therefore be hereby marked "*advertisement*" in accordance with 18 U.S.C. Section 1734 solely to indicate this fact.

[S] The on-line version of this article (available at www.jbc.org) contains Supplemental Figs. S1 and S2 and Tables SI–SIII.

¶ Present address: Juntendo University, Graduate School of Medicine, BioMedical Research Center, 2-1-1, Hongo, Bunkyo-ku, Tokyo 113-8421, Japan.

‡‡ To whom correspondence should be addressed: Tel./Fax: 81-042-367-5709; E-mail: ntakahas@cc.tuat.ac.jp.

[1] The abbreviations used are: FIB, fibrillarin; snRNP, small nuclear ribonucleoprotein; snoRNP, small nucleolar ribonucleoprotein; LC, liquid chromatography; MALDI-TOF, matrix-assisted laser desorption ionization time-of-flight; MS, mass spectrometry; PBS, phosphate-buffered saline; pre-rRNP, preribosomal ribonucleoprotein; RNase, ribonuclease; RNP, ribonucleoprotein; rRNA, ribosomal RNA; SMN, survival motor neuron; RBD, RNA-binding domain; NLS, nucleolar localization signal; NS, SV40 nuclear localization signal.